Improvement of Electrical Conductance on ZnO Nano-Particle Layers for Thin-Film-Transistor Applications with the Use of Thermal Diffusion Type Ga Doping

ISLAM MD MARUFUL
Fujita.Yoshida Laborotory

Submitted in partial fulfillment of the requirements for the degree of Doctor of Engineering at Shimane University.

Supervisor:

Prof. Dr. Yasuhisa Fujita
&
Assistant supervisor:
Prof. Dr. Yasuji Yamada
Prof. Dr. Ryo Sasai &
Assoc. Prof. Dr. Toshiyuki Yoshida

Interdisciplinary Graduate School of Science & Engineering
Shimane University, Japan
March 2022

Acknowledgement

First and foremost, I would like to acknowledge and give my warmest thanks to my supervisors, Prof. Yasuhisa Fujita and Toshiyuki Yoshida, who made this work possible throughout their assistance and insightful advice over the three years of my research. Their research path advise was extremely useful, and it always had a big impact on my ability to improve my study results. I'd like to express my gratitude for their kindness and willingness to contribute their excellent research skills, extensive knowledge, and practical experiences. They constantly helped me understand my study in-depth; for example, they didn't simply show me how to run a research equipment system; they also tried to teach me the core principles of the equipment so that I could increase the quality of my analysis and research findings.

Thank you to Md. Shafiqul Islam and Mr. Raj Deep from “Fujita.Yoshida” laboratory at Shimane University for their enlightening discussions and for making my research and study enjoyable. Thank you very much to Yoshida sensei for his assistance on understanding the principles of NPs synthetization, electrode deposition, and NPs layer characterization using Hall, *I-V*, AFM, SEM, Optical, and XRD system measurements. Next, I'd like to express my gratitude to all of the Shimane University committee members and thesis defense examiners whose questions helped me enhance my study.

Thank you to all of my Shimane University friends, as well as member of “Fujita.Yoshida” laboratory and the “Yeh.Magari laboratory”.

Furthermore, I'd like to express my gratitude to my family, parents, and relatives, who have always been encouraging and supportive of me, even when I wasn't in contact with them on a daily basis.

Declaration

I herewith declared that this dissertation entitled "Improvement of Electrical Conductance on ZnO Nano-Particle Layers for Thin-Film-Transistor Applications with the Use of Thermal Diffusion Type Ga Doping" submitted for the award of a Doctor of Engineering degree by Shimane University that the dissertation was written by myself and that it has not been submitted for any other degree or professional certification. I declare that the work I've submitted is entirely my own and done under the supervision of Prof. Dr. Yasuhisa Fujita, and Assoc. Professor Dr. Toshiyuki Yoshida Department of Physics and Materials Science, Shimane University, Matsue-690-8504. I confirm that appropriate credit has been given to others' work where it has been referenced in this dissertation.

Shimane University *Islam Md Maruful* (seal)
Date:

List of Figures

List of Tables

List of Publications

Journal Article

1) T. Yoshida, **I. M. Maruful**, and Y. Fujita, "Trial of Ga-doping on ZnO nanoparticles by thermal treatment with Ga_2O_3 nanoparticles," *e-Journal Surf. Sci. Nanotechnol.*, vol. 18, pp. 12–17, 2020, doi: 10.1380/EJSSNT.2020.12.

2) **I.M.Maruful**, Toshiyuki Yoshida, and Yasuhisa Fujita. 2022. "Effects of Ambience on Thermal-Diffusion Type Ga-Doping Process for ZnO Nanoparticles" *Coatings* 12, no. 1: 57. https://doi.org/10.3390/coatings12010057**.**

Conference presentation

1) **I. M. Maruful**, T. Yoshida, and Y. Fujita, "Improved current transportation ability of ZnO nanoparticle-based TFTs by diffusion-type Ga-doping" The 4th International Conference on Materials Engineering and Nanotechnology, **ICMEN-2021** Online virtual meeting, Kuala Lumpur, Malaysia.

2) **I. M. Maruful**, T. Yoshida, and Y. Fujita, "Evaluation of ZnO:Ga nanoparticle-based thin-film-transistors" **82nd JSAP Autumn meeting 2021**, Online virtual meeting, Japan.

3) **I. M. Maruful**, T. Yoshida, and Y. Fujita, "study on the thermal-diffusion-type Ga-doping in ZnO nanoparticles aiming for TFT channel application" **67th JSAP Spring meeting 2020**, Online virtual meeting, Sophia University, Tokyo, Japan.

4) **I. M. Maruful**, Yoshida Toshiyuki, Fujita Yasuhisa "Improvement of current transportation ability of ZnO-nanoparticle-based thin-film-transistors by diffusion-type Ga-doping process" 第81回応用物理学会秋季学術講演会　オンライン　2020/9/8-11.

5) **I. M. Maruful**, Atsuya Tabuchi, Toshiyuki Yoshida, and Yasuhisa Fujita, “Trial of the Ga doping to the Sprayed ZnO Nano-Particle Layers by mixing and annealing with Ga2O3”, **第65回応用物理学会春季学術講演会　東京**　2018/3/17-20.

6) 吉田俊幸，**I. M. Maruful**, 藤田恭久「ZnOナノ粒子層伝導特性の向上　～Gaドープの試み～」第79回応用物理学会秋季学術講演会　名古屋　2018/9/18-21.

7) 吉田俊幸，**I. M. Maruful**, 藤田恭久「ZnOナノ粒子層の低抵抗化のための熱拡散型Gaドープにおける熱処理雰囲気の影響」第66回応用物理学会春季学術講演会　東京　2019/3/9-12.

8) 吉田 俊幸, **I. M. Maruful**, 藤田 恭久「ZnOナノ粒子への熱拡散型Gaドープにおける熱処理雰囲気の影響」第80回応用物理学会秋季学術講演会　札幌　2019/9/18-21.

Abstract

The structural, morphological, optical, and electrical properties of Ga-doped ZnO NPs layer prepared by spray-coating method have been studied in this research, concerning two main topics with obtained two significant outcomes.

The 1st main topic is the effect of Ga-doping into ZnO NPs depending on the annealing temperature was investigated. This research focuses on the consequences of annealing temperature on electrical properties. One of the important aspects of this study is the Ga-diffusion mechanism. However, the crystallite size and the orientation of sprayed NPs, both are affected by the annealing with Ga-doping. To confirm the Ga-doping into ZnO, Ga 3d, Zn 3d, and O 1s spectra were analyzed through XPS measurement. The variation of the peak intensity and the energy difference suggested the Ga atoms diffused from Ga_2O_3 into ZnO NPs. The lowest sheet resistance attained 225 Ω/sq in ''Ga_2O_3/ZnO mixed and thermally treated in air''. It was therefore proposed that the NPs annealing at 800°C in our thermal diffusion type Ga-doping process plays an important role to reduce the resistivity of sprayed NPs layer which will improve the electrical conductivity to aim the TFT operation.

The 2nd main topic is the electrical conductivity of Ga-doped ZnO NP layers in terms of structural, optical, and electrical properties in relation to their thermal atmosphere.

Firstly, the structural properties of Ga-doped ZnO NPs layer have been investigated. The Ga-doped ZnO NPs layer deposited on quartz substrates mainly shows high *a*-axis preferred orientation perpendicular to the substrate when deposited at 800°C, while the undoped ZnO shows both poor *c*-axis and *a*-axis orientation identical with lots of defects. Such poor structural properties and defects seriously degrade the performance of electrical conductivity of the NPs layer. The thermally Ga-diffused ZnO NPs samples registered a higher intensity, indicating improved crystallite growth and crystallinity. So, the high-temperature annealing leads to improvement of structural properties, depending on its ambient atmosphere. To understand the effects of these ambient phenomena separately, we employed the open-air, wet-air, dry-air, N_2, and O_2 atmosphere during annealing. It was observed that improving the structure causes the crystallite size to increase and the

crystallite boundary scattering to decrease, resulting in decreased resistivity which leads to the improvement of electrical conductivity of the NPs layer. The electrical conductivity was strongly deteriorated by the crystallite size and the crystallite boundary scattering induced by the inadequate structural properties.

Secondly, optical measurements were used to investigate the progression of the defect mechanism based on the previous findings. The native defects are cause for the degradation of electrical properties and discussed each defect separately by deconvoluting the PL spectra. The Donor-acceptor pair (DAP) emission and the redshift of the exciton emission indicate the successful Ga doping into ZnO NPs.

Thirdly, the electrical properties of Ga-doped ZnO NP layers were investigated depending on the annealing atmosphere. It was found that the electrical conductivity of Ga-doped ZnO NP layers was significantly improved (increased 1000 times or greater) compared to the undoped layer. Using open-air and wet-air atmosphere during annealing, a very low resistivity of $8.0 \times 10^2\,\Omega$/sq and $8.8 \times 10^2\,\Omega$/sq was achieved which improved the current transportation ability between the TFT channel layer. This dramatic variation of sheet resistance is mainly due to the high humidity effect. It had been suggested that humidity is considered to play a key role in enhancing the characteristics of Ga-doped ZnO NPs layers during annealing.

Table of contents

1. Introduction

1.1 Background

The wurtzite structure of ZnO makes it a natural n-type semiconductor. ZnO has grown in popularity as a material for a wide range of device applications during the last few decades. ZnO is nowadays the focus of many studies because of its outstanding properties, such as large exciton binding energy of 60 meV at room temperature, non-toxicity, and low cost. Furthermore, it has the advantage of chemical and thermal stability even in hydrogen plasma atmosphere compared to other oxides used in electronic devices such as SnO_2 and ITO[1]. This enables it to function as a material model, particularly in its wide range of uses (electronics, optics, optoelectronics, conversion photovoltaic)[2],[3]. ZnO in the form of transparent conductive oxides (TCOs) for usage as transparent electrodes has recently received a lot of attention in various applications, especially in optoelectronic devices such as thin-film photovoltaics (TFP)[4], flat panel displays (FPD)[5], and light-emitting diodes (LED)[6,7]. Doping semiconductors is essential for practical applications since it allows to adjust their properties according to demands. Group III, group IIIB rare earth metals, group IV, and group VII elements are all potential n-type dopants for ZnO [8]. Among various doping with ZnO Ga has proven one of the best doping[9] because of reduced chemical reactivity, greater resistance to oxygen, and is less resistance to moisture. Moreover, the radius of Ga^{3+} ions (0.062 nm) is closer to that of Zn^{2+} ions (0.074 nm) than that of Al ions (0.053 nm)[10]. Furthermore, Ga-O (1.92Å) has a shorter covalent bond length than Zn-O (1.97 Å)[10]. As a result, even in the presence of a high Ga concentration, minimal distortion of the doped ZnO lattice occurs.[11]. Gao et al. reported a comprehensive study of doped ZnO using atomic layer deposition (ALD) technique where Ga doped ZnO films showed remarkable enhancement with low resistive NPs layers as well as improved electrical properties[12]. Our study mainly focused on the improvement of electrical conductance on ZnO nano-particle layers aiming for thin-film-transistor applications with the use of thermal diffusion type Ga doping.

1.2 Motivation and strategy

ZnO thin films have been prepared in various technics, such as vacuum arc plasma evaporation (VAPE), magnetron sputtering (MSP), spray pyrolysis, pulsed laser deposition (PLD), evaporation, ion plating (IP), and electrochemical deposition[13], [14]. The thin-film deposition is typically done using high vacuum equipment; however, the upper deposition approach is not suited for our unique Ga doping procedure since Ga doped ZnO NPs are directly sprayed on the substrate to prepare NPs layer. From this compensation, our group developed a physical spray-coating process named "Spray Method" and its highly effective because of its simple, extremely low cost compared to conventional semiconductor, large-area process, broaden selectivity of substrates (materials and surface morphology), etc.[15].

In the spray deposition of ZnO-NPs layers, thickness, structural orientation, defects, and resistivity variation are crucial issues. Our previous group successfully demonstrated both n-type and p-type TFTs, however, the performance of the TFTs declined due to the high resistivity. In this manner, the Ga-doping with ZnO was carried out by thermal diffusion type NPs annealing process to achieve the low resistive ZnO NPs layer to improve the electrical conductivity of the TFT channel layer.

Electrical properties are strongly affected by the doping process depending on its thermal and atmospheric condition. Then there's the issue of determining which component is the most essential in restricting the electrical characteristics of doped ZnO thin films prepared by spray-coating: how do defects and structural qualities affect electrical properties?

Considerable attention has been paid to those issues, the following aspects about Ga-doped ZnO thin films deposited by spray-coating process were addressed in this thesis.

1. The main objective of this study is to clarify the thermal effects of diffusion type Ga-doped ZnO NP layers deposited by the spray-coating method in terms of the electrical, optical, and structural properties. The discussion will especially focus on the resistivity variation of the sprayed NP layers and the Ga diffusion into the ZnO NPs.
2. This study also focused to clarify the ambient effects on the thermal diffusion type

Ga-doped ZnO NPs layer fabricated by the spray-coating method in terms of the electrical, optical, and structural properties. The discussion will focus on the electrical conductivity of TFT channel layer by the consistency of structural, defect, and the transport properties of the thermal diffusion type Ga-doped ZnO NP layers.

1.3 Application and possibilities of semiconducting particle layer

Semiconductor thin films are typically made up of one or more thin layers. Many electronic materials, like transistors, sensors, and photovoltaic devices, are commonly used in such structures. The thickness of semiconductor thin films ranges from a few nanometers to hundreds of micrometers, and their structural, chemical and physical properties are highly correlated to the fabrication technique. In this study, the semiconducting particle layer is directly fabricated using the NPs through coating technics and after obtaining the superior properties, this semiconducting NPs layer can be employed in electronics and optoelectronics devices like transistors, sensors, photovoltaic devices, printed photodetectors, LEDs, solar cells, and so on.

1.4 Scope of the thesis

The evaluation of electrical, morphological, structural, and optical properties of Ga-doped ZnO NPs layers prepared by spray coating deposition technique is described in this thesis. This thesis consists of six chapters.

"Introduction" is the first chapter. This chapter summarizes the study's purpose, which includes all of the study's topics, as well as the thesis's outline.

"Fundamentals" is the second chapter. General properties of zinc oxide (ZnO) are briefly discussed in this chapter, including crystal structure, crystallographic polarity, defects, luminescence in ZnO, and donor-acceptor pair (DAP) emission. Doping elements, thermal and surface conductivity of ZnO, thin-film/layer deposition technics including spray-coating principles, and ZnO-based thin-film transistor (TFT) are also discussed.

"Research Methodology" is the third chapter. The methodology of our novel thermal diffusion type Ga-doping process, the deposition method of NPs layers, and the characterization techniques employed in this dissertation as well as the analytical evaluations have been discussed in this chapter.

The main section of this thesis is divided into two chapters (chapters four and five), each of which contains major themes that have been published (or will be published) in peer-reviewed publications. Each chapter includes an introduction, a description of the experimental procedure, results and discussion, a conclusion, and references.

The fourth chapter is entitled "Ga-doping into ZnO Nanoparticles using Thermal Diffusion Process". The discussion is focused on the changing of the annealing temperature and confirmation of the Ga-diffusion by various measurements.

The fifth chapter is entitled "Optimization of Ambient Atmosphere for Ga-doping and its Application to TFT Channel Layers". The influences of the ambient effects on Ga-doped ZnO NP layers are discussed by the measurement of electrical, structural, and optical properties.

"Concluding Remarks" is the thesis's final chapter. This chapter summarizes the study's results and accomplishments, as well as some concluding notes.

1.5 References

[1] S. Baskoutas, “Special issue: Zinc oxide nanostructures: Synthesis and characterization,” *Materials (Basel).*, vol. 11, no. 6, pp. 11–14, 2018, doi: 10.3390/ma11060873.

[2] A. Srivastava and N. Kumar, “Effect of Post-Deposition Annealing on RF-Sputtered Catalyst-Free Grown ZnO Nanostructures,” *J. Electron. Mater.*, vol. 46, no. 8, pp. 4842–4847, 2017, doi: 10.1007/s11664-017-5443-7.

[3] R. Mimouni, K. Boubaker, and M. Amlouk, “Investigation of structural and optical properties in Cobalt-Chromium co-doped ZnO thin films within the Lattice Compatibility Theory scope,” *J. Alloys Compd.*, vol. 624, pp. 189–194, 2015, doi: 10.1016/j.jallcom.2014.11.016.

[4] M. Karyaoui, A. Ben Jaballah, R. Mechiak, and R. Chtourou, “The porous nature of ZnO thin films

deposited by sol-gel spin-coating technique," *IOP Conf. Ser. Mater. Sci. Eng.*, vol. 28, no. 1, 2012, doi: 10.1088/1757-899X/28/1/012019.

[5] N. Yamamoto *et al.*, "Development of Ga-doped ZnO transparent electrodes for liquid crystal display panels," *Thin Solid Films*, vol. 520, no. 12, pp. 4131–4138, 2012, doi: 10.1016/j.tsf.2011.04.067.

[6] J. K. Sheu, Y. S. Lu, M. L. Lee, W. C. Lai, C. H. Kuo, and C. J. Tun, "Enhanced efficiency of GaN-based light-emitting diodes with periodic textured Ga-doped ZnO transparent contact layer," *Appl. Phys. Lett.*, vol. 90, no. 26, pp. 2005–2008, 2007, doi: 10.1063/1.2753110.

[7] R.-H. Horng, K.-C. Shen, C.-Y. Yin, C.-Y. Huang, and D.-S. Wuu, "High performance of Ga-doped ZnO transparent conductive layers using MOCVD for GaN LED applications," *Opt. Express*, vol. 21, no. 12, p. 14452, 2013, doi: 10.1364/oe.21.014452.

[8] H. Morkoç and Ü. Özgür, *Zinc Oxide: Fundamentals, Materials and Device Technology*. 2009.

[9] Ü. Özgür *et al.*, "A comprehensive review of ZnO materials and devices," *J. Appl. Phys.*, vol. 98, no. 4, pp. 1–103, 2005, doi: 10.1063/1.1992666.

[10] T. H. Chen and T. Y. Liao, "Influence of annealing temperature on the characteristics of Ti-Codoped GZO thin solid film," *J. Nanomater.*, vol. 2013, 2013, doi: 10.1155/2013/502382.

[11] H. Yoon *et al.*, "Effects of Ga concentration on the structural, electrical and optical properties of Ga-doped ZnO thin films grown by sol-gel method," *J. Korean Phys. Soc.*, vol. 64, no. 1, pp. 109–113, 2014, doi: 10.3938/jkps.64.109.

[12] Z. Gao and P. Banerjee, "Review Article: Atomic layer deposition of doped ZnO films," *J. Vac. Sci. Technol. A*, vol. 37, no. 5, p. 050802, 2019, doi: 10.1116/1.5112777.

[13] A. Gide, *Transparent Conductive Zinc Oxide; Basics and Applications in Thin Film Solar Cells*. 1967.

[14] C. J. Kao *et al.*, "Comparison of ZnO metal–oxide–semiconductor field effect transistor and metal–semiconductor field effect transistor structures grown on sapphire by pulsed laser deposition," *J. Vac. Sci. Technol. B Microelectron. Nanom. Struct.*, vol. 23, no. 3, p. 1024, 2005, doi: 10.1116/1.1924613.

[15] D. Itohara, K. Shinohara, T. Yoshida, and Y. Fujita, "P-Channel and n-Channel Thin-Film-Transistor Operation on Sprayed ZnO Nanoparticle Layers," *J. Nanomater.*, vol. 2016, no. Dc, 2016, doi: 10.1155/2016/8219326.

2. Fundamentals

2.1 Zinc Oxide (ZnO)

In recent decades ZnO and its related materials have been a surge in interest to the researchers for a variety of semiconductor device applications. ZnO is a promising material because of its direct band gap of about 3.4 eV and a substantial exciton binding energy of roughly 60 meV at ambient temperature[1]. For optoelectronics application the ZnO materials are considered highly suitable because of its high binding energies. ZnO crystallizes in the same wurtzite form as GaN, however, ZnO is basically form in huge bulk single crystals [2]. Its characteristics have been investigated very beginning of semiconductor technologies[3], but the lack of control over its electrical conductivity has inhibited its usage as a semiconductor in electronic devices. The quality of ZnO single-crystal substrates and epitaxial films has significantly improved during the last decade[4], [5]. As a result, the idea of employing ZnO as an optoelectronic or electronic material by itself has been revived. The possibility of employing ZnO as an alternative or replacement for GaN in optoelectronics has prompted several research organizations throughout the world to emphasize its semiconductor properties, attempting to control inadvertent n-type conductivity and achieve p-type conductivity[6]. Our group has successfully fabricated both n and p-type ZnO NPs by arc-discharge-mediated gas evaporation process and the successful application has been done[7], [8].

2.1.1 Crystal Structure

ZnO has a hexagonal wurtzite crystal shape, which is found naturally as the rare mineral zincite[9][10]. ZnO has a different structure than rock salt, which possesses a metastable cubic phase[11]. The n-type is virtually always present in large bulk single crystals of ZnO[12]. **Fig. 2.1** (a) depicts the Illustration of wurtzite lattice structure of ZnO: *a*-plane, *c*-plane, and *r*-plane. X-ray diffraction revealed the hexagonal unit cell in the crystal structure. The lattice parameters for the *c*-axis and *a*-axis are 5.206Å and 3.25 Å, respectively[11][13]. The lattice parameters of semiconductors are primarily determined by four factors. “(i) The concentration of free electrons, which influences the potential of the conduction band's, which is generally filled by electrons. (ii) Impurity and defect

concentrations, as well as the variation in ionic radii between these defects and impurities and substituted matrix ions. (iii) External strains (such as those caused by the substrate); (iv) temperature"[9]. Another aspect, various imperfections or defects impair the lattice's strict periodicity. These imperfections or defects have a significant and dominating influence on semiconductor mechanical, thermal, electrical, and optical properties. XRD

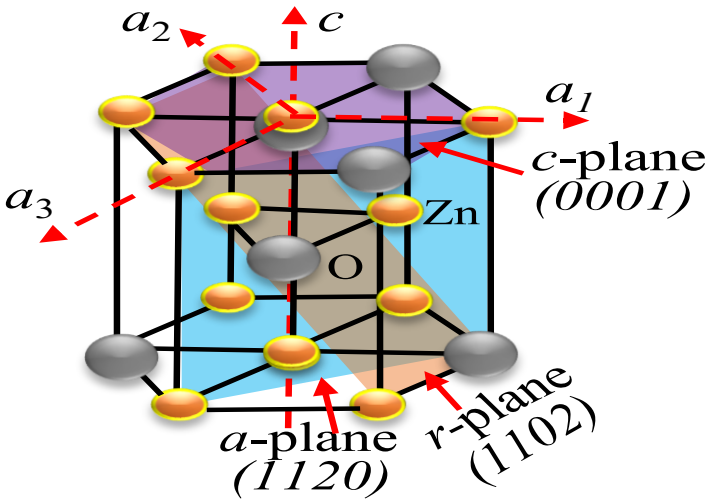

Fig. 2.1 Illustration of wurtzite lattice structure of ZnO: *a*-plane, *c*-plane, and *r*-plane.

measurements can be used in practical studies to estimate the *a*- and *c*-axis lattice constant of ZnO and the volume of the unit cell. The interplanar distance (d) is a value that represents the perpendicular distance between two consecutive planes in a hexagonal *hkl* set and can be calculated by the following equation[14].

$$\frac{1}{d^2} = \frac{4}{3}\left(\frac{l^2+h^2+k^2}{a^2}\right) + \frac{2}{c^2} \quad \text{.....1}$$

where *h*, *k*, and *l* are the miller indices of the plane. The volume of unit cells (V) is calculated using the values of the *a* and *c* lattice constants.

$$V = \frac{\sqrt{3}a^2c}{2} = 0.866a^2c \quad \text{.....2}$$

2.1.2 Polarity of ZnO

There are four major low-index surfaces in ZnO crystals: $(10\bar{1}0)$, $(11\bar{2}0)$, (0001), and $(000\bar{1})$. As previously stated, the latter two are classified as polar since they play an important role in the uses of this material and have distinct chemical properties. Because ZnO has a visible bond, they exhibit a polar character in the *c*-axis direction, which is known as crystal axis polarity. Both two sides faced Zn-polar (0001) and O-polar $(000\bar{1})$ while the other side of *c*-cut ZnO crystals on wurtzite ZnO exhibits a repetition of positively charged Zn^{2+} and negatively charged O^{2-} ions that is perpendicular to the *c*-axis orientation. The difference between the Zn surface (C^+) and the O surface (C^-) polarity produces changes in etching behavior, doping characteristics, defect creation, and growth parameters[15]. Anisotropic electronic structure, mechanical characteristics, and chemical properties are thought to be created by the polarity caused by the spontaneous polarization of ZnO[16]. **Fig. 2.2** demonstrates how ZnO crystallizes into the wurtzite structure, which mainly consists of Zn and O atoms alternating planes along the *c*-axis. [17], [18].

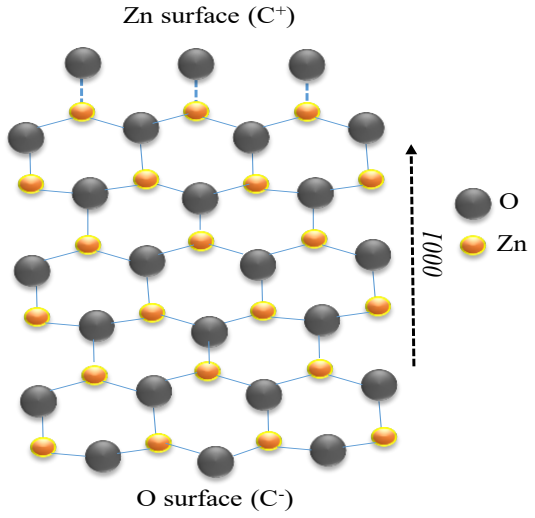

Fig. 2.2 Atomic arrangements of Zn (*0001*) and O ($000\bar{1}$) polar surface to the c-axis in a wurtzite structure of ZnO.

2.1.3 Defects in ZnO

Although ZnO presents several benefits for optoelectronics and electronics device application, doping & defect control, which are key features for device applications, remain a major concern. Impurities and defects can control the electrical and optical characteristics of ZnO. The impurity doping element such as Gallium (Ga), Aluminum (Al), Indium (In), and Hydrogen (H) can sometimes be donor type, or of the acceptor type, such as Phosphorus (P), Arsenic (As), Antimony (Sb), and N[19]. The performance and properties of ZnO and doped ZnO are significantly influenced by native point defects. Acceptor defects, such as zinc vacancies (V_{Zn}) and oxygen interstitial (O_i), differ from donor defects, which include zinc interstitial (Zn_i) and oxygen vacancies (V_O). O vacancy, Zinc interstitial, and Zn antisite, which are related to O deficiency or the overabundance of Zn, are donor-type defects. The V_{Zn}, O_i, and Oxygen antisite are acceptor-type defects related to Zn deficiency or the overabundance of Oxygen[20].

Although the Zn_i is described as a shallow donor[21], it is extremely motile[12] and unstable in an open atmosphere[22]. As a result, the ZnO has been annealed out at a temperature of 170 K [23]. The V_O counts as a deep level donor in n-type ZnO and cannot be considered a source of negative carriers, whereas the Zn vacancy counts as a deep acceptor and cannot be considered a substantial source of holes. First-principles studies[24] have confirmed the deep donor properties of V_O. Despite the fact that V_O is a deep donor, its formation energy is lower[25] than Zn_i, which is a shallow donor in ZnO[20]. Compared to all other native defects in n-type ZnO, the V_{Zn} is considered to be the most significant deep level acceptors, having the lowest formation energy.

In addition, Impurities play a major role in native point defects such as V_O and Zn_i. Instead of point defects and other impurities, hydrogen diffusion could occur on the ZnO crystal. According to reference No. 19, when the formation energy is minimal, H is indeed a donor in ZnO and is immediately ionized. Based on a theoretical investigation, in n-type ZnO H is anticipated as a shallow donor. According to first-principal calculations, H can occupy an O substitutional site and behave as a shallow donor[24]. Furthermore, group III elements as a dopant highly interact with native defects and H may affect the electrical properties of ZnO. Native defect complexes with donor elements have been suggested by

Look et, al. it should emerge in n-type ZnO and contribute to its conductivity [26]. The introduction of impurities during the growth or annealing process can be used to regulate native point defects[21]. In practical research, native defects of ZnO can be detected using spectroscopic measurements such as photoluminescence (PL); nevertheless, the significance of native point defects is yet uncleared.

2.1.4 Luminescence in ZnO

ZnO is a good material based on its applications of phosphor technology because of its intense luminosity in the green and white portions of the spectrum. The spectra feature a broad emission peak at 495 nm [half-width of 0.4 eV] [27]. ZnO is highly suitable for usage in vacuum fluorescent displays and field emission displays because of its n-type conductivity[9]. Single crystals, thin films/layer and threads, nanocrystals, needles, and other forms of ZnO have two luminescence bands: "a short-wavelength band near the crystal's absorption edge, i.e., band-edge luminescence, and a broader long-wavelength band, the maxima of which is typically in the green spectral range called green luminescence" [31]. The existence of luminescence band structure of ZnO showed in **Fig. 2.3**.

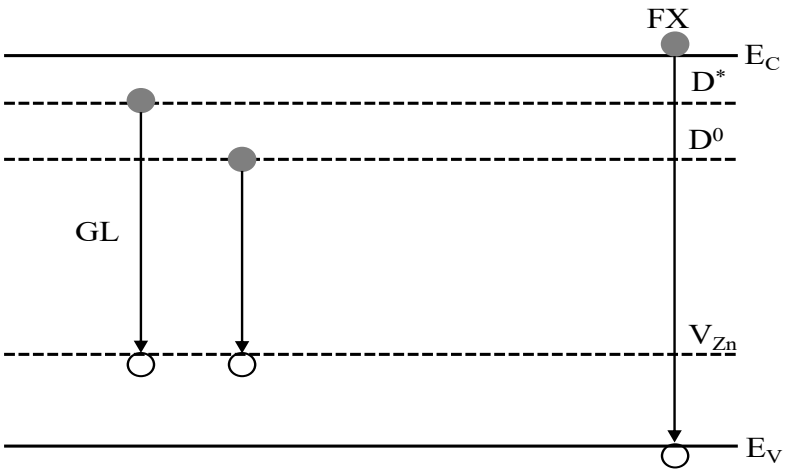

Fig. 2.3 The band structure of ZnO with Green and the band-edge luminescence mechanism.

2.1.4.1 Green Luminescence

Despite a large number of investigations, the nature of green luminescence still remains unknown. Considering basic models of green luminescence and possible luminescence centers, excluding implausible candidates in ZnO such as zinc interstitial (Zn_i) (known as shallow donor) and oxygen anitisites, which have high formation energy. Few study stated that the copper ions replace the zinc ions which mainly occur in a small portion in ZnO, creating the green luminescence band with a maximum at λm = 535 nm (2.32 eV) and FWHM E1/2 = 330 meV[28], [29]. Electronic transitions involving shallow donors and deep level acceptors (V_{Zn}) generate green luminescence in ZnO, as shown in[30], [31], and the green band in ZnO behaves in a similar way to the yellow band in GaN. The appearance of regularly spaced maximum at the short-wavelength edge of the green luminescence band at helium temperatures is linked to the existence of two types of shallow donors in ZnO with depths of 30 and 60 meV.[30]. This model was later improved. Thin (300 nm) zinc oxide films containing nitrogen were utilized in the experiment (ZnO:N)[31]. The intensity of green luminescence showed an unusual temperature dependence: the luminescence intensity increased as the sample temperature climbed from 15 to 50 K[31]. An examination of the data obtained came to the conclusion that, rather than two types of shallow donors, there is only a single type of shallow donor with 2 phases, the ground level, and the exciting level. According to the reference No. 31, Electronic transitions between the ground (D^0) and the excited (D^*) states of the shallow donor's to the deep acceptor (V_{Zn}) induce the green illumination[31].

2.1.4.2 Edge Luminescence

The edge luminescence exhibits an excitonic characteristic, with a maximum at 3.35 eV and a decay period of 0.7 ns[32]. Edge luminescence has a sub-nanosecond deexcitation period, making it particularly useful for high-speed systems (lasers, scintillators, phosphors). Edge luminescence involves free excitons (FXs), excitons associated with acceptors and donors and related two-electron orbits, donor-acceptor coupling, and phonon replicas. Reference[32] describes in detail the entire range of lines that pertain to the centers mentioned above.

2.1.4.3 Interrelation between Green and Edge Luminescence:

The proponents of both the model of V_{Zn}[31] and the model of V_O[33] for green luminescence centers have noticed that green luminescence is linked to edge luminescence. The basic radiative transitions in ZnO are shown in **Fig. 2.3**, with V_{Zn} serving as luminescence centers. As previously stated, electronic transitions from the ground (D^0) and excited (D^*) states of a shallow donor to a deep acceptor (V_{Zn}) which mainly causes from green luminescence[25]. Energy transfer from excitons to V_O happens in ZnO samples and in the form of oxygen vacancies. Green luminescence exciton spectrum shows in a longer wavelength (broad band) is about 3.5 eV and a halfwidth of 300 meV, as well as strong peaks in the region of bound excitation energy is about 3.35 eV[34].

2.1.4.4 Donor-acceptor pair (DAP) emission

Semiconductors are frequently doped by both donor and acceptor impurities, either purposefully or inadvertently. This is common in Integrated Circuit (IC) manufacturing, an n-type doping is commonly performed by substituting a larger concentration of donor impurities for the p-type acceptor impurities. In this instance, the majority of the acceptors will be ionized by donor electrons rather than valence band electrons, ensuring that neither impurity contributes to the free carrier population as shown in **Fig. 2.4**. These contaminants in the donor and acceptor have adequately compensated for each other. Electrons can be trapped and form neutral donors (D^0), and holes can be trapped and form neutral acceptors (A^0) if the semiconductor is optically stimulated or carriers are introduced at very low temperatures[35]. Most of these sites will produce donor-acceptor pair (DAP) excitons with their nearby complementary impurity in a properly compensated (about equal D and A concentrations) sample, and these excitons can efficiently luminesce. In semiconductors, excited electrons and holes can take a variety of forms, ranging from basically free in high-quality high-temperature crystals to densely bound excitons (electron-hole pairs) in disorganized or molecular systems.[36]. A key light-emission mechanism in ZnO is the donor-acceptor-pair (DAP) transition in II-VI and III-V semiconductors. Another acceptor-related luminescence (DAP luminescence) in ZnO has been seen such as acceptor bound excitons[37] and free-electron acceptor

recombination[38].

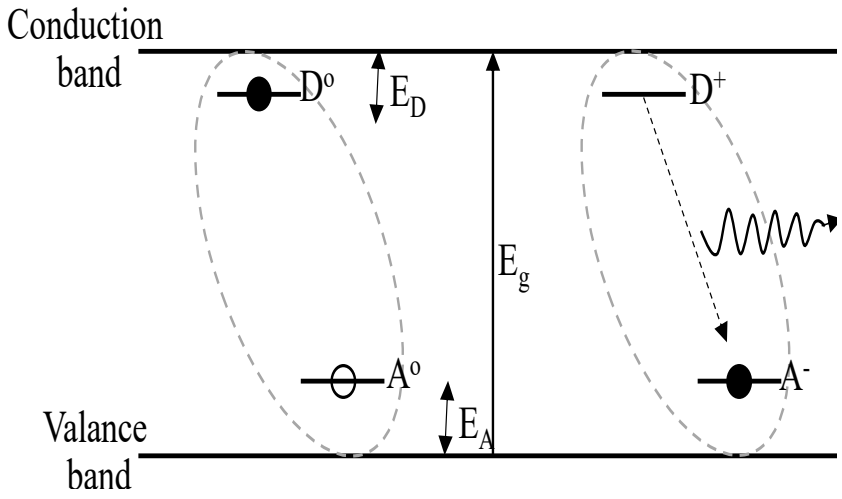

Fig. 2.4 Electronic energy structure of acceptor impurities and shallow donor in a semiconductor.

Thonke et al. found a 3.232 eV peak in the luminescence spectra of ZnO, which they attributed to a DAP transition, and the acceptor in the DAP transition was attributed to being N_O (nitrogen replacing on an oxygen site)[32]. According to Wang et al., when the temperature rises, the DAP peak position raises from 3.229 eV at 10 K to 3.246 eV at 100 K, (blue shift) then drops[39]. As the measurement temperature rises, the blue shift is attributed to an increase in free-electron-to-acceptor (FA) emission due to shallow donor activation and the red shift is due to the DAP effect. The peak positions of such two phonon counterparts have likewise been observed blue shift as the temperature rises. [39]. The zero phonon line (ZPL) was determined at 2.8505 eV in defect emission, and the relative intensity of the n^{th} phonon was estimated using the relation. [40].

$$I_n = I_0(s^n e^{-S}/\mathrm{n!}) \quad \ldots\ldots\ldots\ldots\ldots\ldots 3$$

In this relation, the S is called Huang Rhys factor and the value of green band related Huang Rhys factor S ≈ 6.8 was estimated by [30].

$$S = \frac{e^2}{\sqrt{2\pi}\cdot a_b \hbar\omega_{LO}} \frac{1}{\left(\frac{1}{\varepsilon_\infty} - \frac{1}{\varepsilon_S}\right)} \; or \; S = \frac{E_r}{\hbar\omega_{LO}} \quad \ldots\ldots\ldots\ldots\ldots\ldots\ldots\ldots 4$$

ZnO DAP band edge related Huang Rhys factor S is 0.62 and estimated by[32].

$$S = E_A \frac{2\varepsilon_S}{2\pi\cdot\hbar\omega_{LO}} \frac{1}{1/2\left(\frac{1}{\varepsilon_\infty} - \frac{1}{\varepsilon_S}\right)} \quad \ldots\ldots\ldots\ldots\ldots\ldots\ldots\ldots 5$$

2.1.5 Thermal conductivity of ZnO

As a result of this feature, ZnO can be used as an additive material to improve the thermal conductivity of a semiconductor device. This also makes ZnO a more appealing substrate for homoepitaxy or heteroepitaxy (for example, growth of GaN, which has a comparable lattice constant)[41], [42]. When the device is in use, it has excellent thermal conductivity, which leads to a high heat extraction efficiency. The majority of the studies focused on ZnO NPs but the thermal conductivity is extremely low at ambient temperature[43]. Later on, the availability of higher-quality bulk ZnO samples resulted in higher thermal conductivity measurements, owing to greater sample quality[4]. Florescu et al. examined the thermal conductivity of bulk n-type ZnO developed by vapor-phase transport in the [0001] plane at ambient atmosphere and observed values ranging from 98–116 W/mK[41]. For bulk ZnO the thermal conductivity was utilized using obtained technique following various thermal treatments, reporting values in the range from 46 to 147 W/mK at ambient atmosphere[42]. Although interface scattering is predicted to dominate phonon transport in compacted powder, the thermal conductivity revealed a definite 1/T temperature dependency from those sintered samples, indicating that a harmonic phonon scattering is dominant, as found in perfect or improvement of crystals. As a result, sintering is quite likely to have aided the development of polycrystalline ZnO with larger crystals[44].

2.1.6 Surface conductivity of ZnO

The conductivity of ZnO thin films is highly dependent on the surface's exposure to a variety of gases. It's previously been reported that sheet resistance of ZnO is micro-ohm ($10^{-4}\ \Omega^{-1}$) and has a good surface conductivity that is responsible for improved current conduction ability. It's mostly exposed to UV without heating above the band gap or by overheating above 500°C in a vacuum[45]. This conductive layer is quenched by exposure to oxygen, especially in the presence of humidity. According to reference No. 46, the molecular oxygen atoms were thought to behave as acceptors, trapping electrons in a negative surface charge layer near the surface of a typical n-type crystal, resulting in a depletion zone and reduced conductivity. Because the sample thickness is much greater than the thickness of any depletion region, the size of the depletion region by itself is insufficient to compensate for the conductivity reduction. Defects with a higher density towards the surface could generate the layer such as oxygen vacancies, which could have been caused by illuminance[46]. UV exposure was discovered to cause faults with the same Electron Paramagnetic Resonance (EPR) signal as CO exposure and subsequent CO_2 desorption[46].

2.2 doping of ZnO

The doping concentration is critical to control the purposefully added impurities, which are liable to stable the ZnO electrical properties, in order to develop any form of device technology. Ambipolar doping is the main issue in using ZnO as a semiconductor for electro-optic devices. This difficulty is common in broad band gap materials, in which doping of n-type is easy to achieve up to high densities but doping of the p-type is difficult. ZnO is naturally an n-type semiconductor[47]. Many studies have concentrated on modifying ZnO's physicochemical characteristics to fulfill specific of a specific applications, which is crucial for improving the performance of innovative devices. Because defect chemistry plays an important role in optoelectronic applications, it is well accepted that the characteristics are highly reliant on the impurity level.[48], [49]. As a result, doping was initially a highly useful approach to adjust the electrical and optical properties of ZnO. Group III elements (Al, In, Ga) have higher energy states and can

closely merge with conduction band levels and create free electrons to occupy the conduction band when doping with ZnO [23], [50], [51]. Ga^{3+} has been attracting attention among these dopants because of its inexpensive cost, lack of toxicity, and high closeness between the ionic radii of Ga^{3+} (0.61) and Zn^{2+} (0.74)[52]. Because of its high carrier concentration and electrical conductivity, Ga-doped ZnO (often abbreviated as GZO) is a particularly attractive material for a variety of novel applications[53],[54]. However, in contrast to doping, the microstructural characteristics of ZnO, such as crystal size, crystal orientation, aspect ratio, crystalline density, surface volume, surface morphology, and so on, have a considerable impact on the electrical and optical properties of the material[55]. From this sense, the structural and optical properties were studied with the thermal diffusion type Ga-doped ZnO NPs layer. Among numerous doping technologies, it's an innovative and simple process, notably for doping with NPs.

2.3 Thermal diffusion into ZnO

The thermal diffusion process is mainly due to the relative motion of the mixture by the temperature gradient. A concentration gradient occurs in the mixture as a result of this motion, and an ordinary diffusion is formed to eliminate the gradient. When the mass flux of each species is zero in the stationary state, the thermal diffusion factor and thermal conductivity of a binary mixture are defined as[56]

$$\alpha T = -\frac{T}{x_1 x_2}\left(\frac{\nabla x_1}{\nabla \mathrm{T}}\right) \quad \text{.....6}$$

Where x1 and x2 is the mole function of the component for 1 and 2,

∇T and ∇x_1 are gradients of temperature and mole fraction of heavier components, and T is the temperature.

In general, thermal diffusion and ion implantation are well-known methods for impurity doping. For isolating the chemical reaction of diffusion in an atmosphere free of impurity components, highly pure gases such as $POCl_3$ and N_2, O_2, and others are utilized. Thermal diffusion in a normal environment could function as well as the conventional method if a method can prevent the silicon surface from the penetration of various contaminates while allowing only the targeted substance to diffuse in the silicon surface in some way. The ion implantation is basically used in high vacuum technology during thin-film

deposition[57]. Thermal diffusion is often used in nanofluid technology to induce the dopant[57]. In our thermal diffusion process used oxide NPs to introduce the impurity doping by diffusion mechanism. The Ga_2O_3 and ZnO NPs directly annealed using furnace temperatures ranging from 600~1000°C and the Ga^{3+} atoms occupied into the Zn^{2+} sites through a thermal diffusion mechanism. According to reference no. [58], for gallium diffusion, two models are proposed: one based on the interstitialcy (kick-out) mechanism and the other on the vacancy mechanism. The mechanism of interstitialcy (kick-out) is stated as follows:

$$Ga_i^{-} \rightarrow Ga_{Zn}^{+} + I_{Zn}^{2-} \quad \ldots\ldots\ldots\ldots\ldots\ldots 7(a)$$

$$\rightarrow Ga_{Zn}^{+} + I_{Zn}^{0} + 2e \quad \ldots\ldots\ldots\ldots\ldots 7(b)$$

The vacancy mechanism stated as follows

$$(Ga_{Zn} + V_{Zn})^{-} \rightarrow Ga_{Zn}^{+} + V_{Zn}^{2-} \quad \ldots\ldots\ldots\ldots\ldots 8(a)$$

$$\rightarrow Ga_{Zn}^{+} + V_{Zn}^{0} + 2e \ldots\ldots\ldots\ldots\ldots 8(b)$$

According to the theories above, the gallium diffusion zone in ZnO is an n-type semiconductor. Furthermore, it was assumed that donors diffused through zinc vacancies in ZnO[22]. Considering the previous studies, the most likely diffusion model for gallium in ZnO is the zinc vacancy-mediated mechanism shown in eq. (8).

2.4 Film/Layer deposition technics

In thin-film/layer deposition techniques, vacuum-based and solution-based deposition are the most frequent processes. Physical Vapor Deposition (PVD) and Chemical Vapor Deposition (CVD) are the two most used vacuum-based deposition methods in thin-film deposition technology[59]. Although solution-based deposition techniques are cost-effective and simple to utilize, they also have significant drawbacks. Several factors, such as cost, purity, and porosity, must be addressed while choosing the best fabrication method for a certain application.

2.4.1 Physical Vapor Deposition (PVD) technic

PVD is called a physical vapor deposition method, it is generally classified into vacuum

deposition[59], sputtering[60], and ion plating[61]. These are vacuum low-temperature film formation technologies, and the film formation is due to the vaporized gas or sputtered particles in the vacuum of the film raw material, so basically there is no need to heat the processed material. Therefore, it is characterized by a wide range of applicable base materials and a smooth surface of the obtained film.

2.4.2 Chemical Vapor Deposition (CVD) technic

CVD is a process that uses gas-phase sources to produce thin layers on the substrate surface through chemical reactions. When the source gases are injected into the reaction chamber, the diffusion mechanism happen into the surface layer inside the chamber and forms the thin layer by a chemical reaction between the numerous gas atoms and the substrate. Plasma assisted CVD uses active ions that appear in the plasma. Vacuum evaporation and molecular beam epitaxy (MBE)[62], spray pylorosis[34], are based on the Thermal process. Temperatures in the range of 600 to 1100°C are being used in CVD coating procedures. Significant thermal impacts on the substrate material are possible at these high temperatures.

2.4.3 Spray-coating method

Because the annealed NPs are directly deposited onto the substrate with solution-based deposition technics in our thermal diffusion type Ga-doping technique, the aforementioned coating technique is vacuum-based deposition technics and is highly appropriate for thin-film fabrication. In this way, our group developed physical spray-coating techniques for NPs layer fabrication, named the "spray" method. Because of its incredibly low cost compared to conventional semiconductor processes, large-area process, broaden selectivity of substrates (materials and surface morphology), our spray-coating is simple and cheapest compared with other solution-based deposition techniques. In this method, sintering of the particles takes time and agglomerates, and it is manufactured by a spray method using an airbrush. The general spraying method may be carried out in atmospheric gas or reduced atmosphere pressure, but in this study, it is carried out under atmospheric pressure. First by increasing the temperature of the hot plate by keeping the amount to be sprayed constant, the sprayed ZnO nanoparticle

dispersion to form a nanoparticle layer by adjusting the temperature of the hot plate. At this time, though it is thought that suppression of the amount of evaporation of nitrogen can be achieved. Due to the deposition of NPs layer in the atmospheric ambient, the defect can arise on the NP surface and the defect properties are discussed in section four.

2.5 Oxide Semiconductor Thin-Film Transistors (TFTs)

Oxide TFTs, have been gaining a lot of attention since 2003, when the first reports on ZnO TFTs, particularly InGaZnO TFTs, were reported[63]. Because of its potential features, such as high mobility at low processing temperatures, low fabrication cost, and superior transparency, oxide semiconductors have recently been actively explored. Additionally, oxide TFTs have various advantages over traditional a-Si TFTs, including transparency in the visible region, high field-effect mobility, controlled turn-on voltage, and high subthreshold swing[64]. Oxide thin film deposition with good uniformity and smooth surface at low temperatures helps to expand the possible applications for a-oxide semiconductor TFTs, such as in big areas, transparent displays, or flexible devices. Oxide-TFTs are extremely simple to build into devices, in addition to their superior qualities. Because a-Si reacts readily with O_2 in air, the manufacturing of a-Si TFTs necessitates a closed system and, in most cases, a vacuum. Despite this, Oxide-TFTs can be manufactured in an open system at ambient pressure. TFTs and circuits-based devices have a wide range of applications based on the structure, the most prominent of which is undoubtedly flat panel displays. A viable technique is enabled by amorphous, polycrystalline, and microcrystalline silicon. Channel mobility of ≤ 1 cm^2/Vs and $I_{ON/OFF}$ $\geq 10^6$ are typical performance values[64], [65]. Higher performance, reduced fabrication temperatures, transparency, and flexible substrates are all advantages of oxide-based devices.

2.5.1 In-Ga-Zn-O (IGZO) TFTs

Metal oxide semiconductor thin-film transistors (TFTs), particularly those based on indium–gallium–zinc–oxide (IGZO), have attracted a lot of attention since Nomura et al,

demonstrate the first amorphous IGZO TFT (a-IGZO) in 2004[63]. Crystalline IGZO materials were initially reported in 1985, before the development of the first a-IGZO-based TFT[66]. However, Instead of amorphous and single-crystalline of IGZO, Nomura et al. used in other materials as IGZO-TFT channel layer until 2004[63]. Single-crystalline TFTs have the advantage of having no surface defects, resulting in ultra-high mobility TFTs. On the other hand, single-crystal development necessitates a high temperature, which is inconvenient for large-area applications. In 2004, Nomura et al. presented the first confirmation that a-IGZO films could be produced at low temperatures. [67]. The most popular TFT channel semiconductor materials are now a-IGZO films. a-IGZO-based TFTs typically have field-effect mobility greater than 10 $cm^2/(V.s)$ when compared to amorphous silicon TFTs, the mobility is less than 1.0 $cm^2/(V.s)$[68], [69] but nowadays for high-resolution display or high speed transistor application, the mobility is insufficient. IGZO-based TFTs have been proved to have various potential uses in liquid crystal displays (LCDs), organic light-emitting diodes (OLEDs), and electronic paper displays by several well-known display makers, sensor technology, various applications in addition to flat panel displays (FPD) [70]. The major advantages of IGZO-based TFTs are distinct light sensitivity, pressure sensitivity, pH sensitivity, gas sensitivity, and a few other parameters which are important for these sensors. Moreover, it's easier to implement sensors with IGZO-TFTs because of the relatively developed display technology. Because of their superior properties like, light weight, ultrathin thickness, and mechanical bend resistance, IGZO-based TFTs have a lot of potentials in particular the field of flexible electronics[71].

2.5.2 ZnO-based Metal-Semiconductor Field Effect Transistor (MESFET)

The MISFET principle is used in most oxide-based TFTs, which consists of a gate contact with an insulating layer, with top or bottom gate electrode. While this method has shown to be very useful in silicon technology because of the low defects at the Si/SiO_2 interface and the low leakage current. The dielectric thickness in oxide MISFETs is typically 50-200 nm. MESFETs are less complicated and less expensive. In reality, the gate insulator's growth is critical for MISFET performance and necessitates a great deal

of effort in growth procedures. To ensure minimal leakage currents, the insulator thickness must be quite thin (in the region of 100 nm). Because a considerable portion of the applied gate voltage is lost across this thick insulator, the MISFETs can operate at high operating voltages of 10 V or higher. MESFETs have a higher gain when the gate voltage is between 1 and 3 V.[72]. MESFETs have the most significant benefit over MISFETs due to the absence of an insulator-semiconductor interface: channel mobility is greater due to fewer interface traps with which electrons can scatter. Furthermore, unlike MISFETs, the effects of visible light and voltage stress do not affect the threshold voltage of MESFETs. MESFETs have channel mobility equal to the bulk mobility of their individual semiconductor, which is much higher than most MISFETs' field-effect mobility[73]. Based on the above circumstances we demonstrated the ZnO metal-semiconductor field-effect transistor (MESFET) discussed in this study.

Mead proposed and demonstrated the MESFET for the first time in 1966[72]. A metal-oxide-semiconductor field-effect transistor (MOSFET) is very similar to a MESFET[74]. The fundamental distinction is that a metal-semiconductor (Schottky) junction replaces the MOS gate in a MESFET. Highly rectifying Schottky contacts such as Ag, Pt, Pd, or Au deposited on thin ZnO channels by reactive DC-sputtering to make ZnO-based MESFETs. Lajn et al. revealed that Metals, with the exception of Au, are partially oxidized on ZnO thin films, [75]. ZnO-MESFETs are made on glass substrates that are more industrially relevant. The conductivity of MESFET channels on quartz glass vs two commercial borosilicate substrates differs significantly. Quartz has channel mobility of about 1.3 cm^2/Vs and the highest on/off ratio of about $4.7x10^5$[77]. MESFETs on borosilicates have channel mobilities that are one to two decades lower. This means that the gate material's oxidation has changed[77]. For the low voltage operation, the MESFET is widely used in microwave applications. The operation of MESFET is described in section four with detailed characterization.

2.6 References

[1] Y. Chen *et al.*, “Plasma assisted molecular beam epitaxy of ZnO on c-plane sapphire:

Growth and characterization," *J. Appl. Phys.*, vol. 84, no. 7, pp. 3912–3918, 1998, doi: 10.1063/1.368595.

[2] D. C. Reynolds, D. C. Look, and B. Jogai, "Optically pumped ultraviolet lasing from ZnO," *Solid State Commun.*, vol. 99, no. 12, pp. 873–875, 1996, doi: 10.1016/0038-1098(96)00340-7.

[3] Harvey E Brown; New Jersey Zinc Company, *Zinc oxide rediscovered.* New York: New York, NY : New Jersey Zinc Company, 1957.

[4] Ü. Özgür *et al.*, "A comprehensive review of ZnO materials and devices," *J. Appl. Phys.*, vol. 98, no. 4, pp. 1–103, 2005, doi: 10.1063/1.1992666.

[5] E. T. Robert Triboulet, Vicente Munoz-Sanjosé, Ramon Tena-Zaera, Mari Carmen Martinez-Tomas (auth.), Norbert H. Nickel, *Zinc Oxide — A Material for Micro- and Optoelectronic Applications*. Springer Netherlands, 2005.

[6] Chennupati Jagadish Stephen Pearton, *Zinc Oxide Bulk, Thin Films and Nanostructures*. Elsevier Science, 2006.

[7] Y. Fujita, K. Moriyama, Y. Hiragino, Y. Furubayashi, H. Hashimoto, and T. Yoshida, "Electroluminescence from nitrogen doped ZnO nanoparticles," *Phys. Status Solidi Curr. Top. Solid State Phys.*, vol. 11, no. 7–8, pp. 1260–1262, 2014, doi: 10.1002/pssc.201300645.

[8] D. Itohara, K. Shinohara, T. Yoshida, and Y. Fujita, "P-Channel and n-Channel Thin-Film-Transistor Operation on Sprayed ZnO Nanoparticle Layers," *J. Nanomater.*, vol. 2016, no. Dc, 2016, doi: 10.1155/2016/8219326.

[9] J. Zemann, " Crystal structures, 2 nd edition, Vol. 3 by R. W. G. Wyckoff ," *Acta Crystallogr.*, vol. 21, no. 3, pp. 455–455, 1966, doi: 10.1107/s0365110x6600327x.

[10] H. Morkoç and Ü. Özgür, *Zinc Oxide: Fundamentals, Materials and Device Technology*. 2009.

[11] A. Gide, *Transparent Conductive Zinc Oxide; Basics and Applications in Thin Film Solar Cells*. 1967.

[12] A. Janotti and C. G. Van De Walle, "Fundamentals of zinc oxide as a semiconductor,"

Reports Prog. Phys., vol. 72, no. 12, 2009, doi: 10.1088/0034-4885/72/12/126501.

[13] Z. Zno, Z. Zno, and Z. Zno, "rl," vol. lxxxviii, no. April, 1913.

[14] John Wiley & Sons, *Solid State Chemistry and its Application*. 2014.

[15] E. Klingshirn, C. & Meyer, B. & Hoffmann, A. & Geurts, J. & Wagner, Markus & Malguth, *Zinc Oxide: From Fundamental Properties Towards Novel Applications.* 2010, page 7-37.

[16] J. R. Williams *et al.*, "Observation and simulation of hard x ray photoelectron diffraction to determine polarity of polycrystalline zinc oxide films with rotation domains," *J. Appl. Phys.*, vol. 111, no. 3, 2012, doi: 10.1063/1.3682088.

[17] M. W. Allen *et al.*, "Polarity effects in the x-ray photoemission of ZnO and other wurtzite semiconductors," *Appl. Phys. Lett.*, vol. 98, no. 10, pp. 2011–2014, 2011, doi: 10.1063/1.3562308.

[18] R. Wahl, J. V. Lauritsen, F. Besenbacher, and G. Kresse, "Stabilization mechanism for the polar ZnO(000$\bar{1}$)-O surface," *Phys. Rev. B - Condens. Matter Mater. Phys.*, vol. 87, no. 8, pp. 1–12, 2013, doi: 10.1103/PhysRevB.87.085313.

[19] D. C. Look, "Progress in ZnO materials and devices," *J. Electron. Mater.*, vol. 35, no. 6, pp. 1299–1305, 2006, doi: 10.1007/s11664-006-0258-y.

[20] F. Oba, M. Choi, A. Togo, and I. Tanaka, "Point defects in ZnO: An approach from first principles," *Sci. Technol. Adv. Mater.*, vol. 12, no. 3, 2011, doi: 10.1088/1468-6996/12/3/034302.

[21] D. C. Look, J. W. Hemsky, and J. R. Sizelove, "Residual native shallow donor in ZnO," *Phys. Rev. Lett.*, vol. 82, no. 12, pp. 2552–2555, 1999, doi: 10.1103/PhysRevLett.82.2552.

[22] P. Erhart and K. Albe, "Diffusion of zinc vacancies and interstitials in zinc oxide," *Appl. Phys. Lett.*, vol. 88, no. 20, 2006, doi: 10.1063/1.2206559.

[23] M. D. McCluskey and S. J. Jokela, "Defects in ZnO," *J. Appl. Phys.*, vol. 106, no. 7, 2009, doi: 10.1063/1.3216464.

[24] A. Janotti and C. G. Van De Walle, "Oxygen vacancies in ZnO," *Appl. Phys. Lett.*, vol. 87,

no. 12, pp. 1–3, 2005, doi: 10.1063/1.2053360.

[25] A. Janotti and C. G. Van De Walle, “Native point defects in ZnO,” *Phys. Rev. B - Condens. Matter Mater. Phys.*, vol. 76, no. 16, pp. 1–22, 2007, doi: 10.1103/PhysRevB.76.165202.

[26] D. C. Look, G. C. Farlow, P. Reunchan, S. Limpijumnong, S. B. Zhang, and K. Nordlund, “Evidence for native-defect donors in n-type ZnO,” *Phys. Rev. Lett.*, vol. 95, no. 22, pp. 1–4, 2005, doi: 10.1103/PhysRevLett.95.225502.

[27] M. J. Weber, a V Dotsenko, L. B. Glebov, and V. a Tsekhomsky, *Handbook of Phosphors*, vol. 23, no. 1. 2003.

[28] R. Dingle, “Luminescent transitions associated with divalent copper impurities and the green emission from semiconducting zinc oxide,” *Phys. Rev. Lett.*, vol. 23, no. 11, pp. 579–581, 1969, doi: 10.1103/PhysRevLett.23.579.

[29] Y. I. Alivov, M. V. Chukichev, and V. A. Nikitenko, “Green Luminescence Band of Zinc Oxide Films Copper-Doped by Thermal Diffusion,” *Semiconductors*, vol. 38, no. 1, pp. 31–35, 2004, doi: 10.1134/1.1641129.

[30] D. C. Reynolds, D. C. Look, and B. Jogai, “Fine structure on the green band in ZnO,” *J. Appl. Phys.*, vol. 89, no. 11 I, pp. 6189–6191, 2001, doi: 10.1063/1.1356432.

[31] P. A. Rodnyi and I. V. Khodyuk, “Optical and luminescence properties of zinc oxide (Review),” *Opt. Spectrosc. (English Transl. Opt. i Spektrosk.*, vol. 111, no. 5, pp. 776–785, 2011, doi: 10.1134/S0030400X11120216.

[32] B. K. Meyer *et al.*, “Bound exciton and donor-acceptor pair recombinations in ZnO,” *Phys. Status Solidi Basic Res.*, vol. 241, no. 2, pp. 231–260, 2004, doi: 10.1002/pssb.200301962.

[33] F. H. Leiter, H. R. Alves, A. Hofstaetter, D. M. Hofmann, and B. K. Meyer, “The oxygen vacancy as the origin of a green emission in undoped ZnO,” *Phys. Status Solidi Basic Res.*, vol. 226, no. 1, pp. 5–6, 2001, doi: 10.1002/1521-3951(200107)226:1<R4::AID-PSSB99994>3.0.CO;2-F.

[34] T. M. Børseth, B. G. Svensson, A. Y. Kuznetsov, P. Klason, Q. X. Zhao, and M. Willander, “Identification of oxygen and zinc vacancy optical signals in ZnO,” *Appl. Phys. Lett.*, vol. 89, no. 26, pp. 1–4, 2006, doi: 10.1063/1.2424641.

[35] K. W. Böer and U. W. Pohl, Carriers in Magnetic Fields and Temperature Gradients, *Semiconductor Physics*. 2020, doi:10.1007/978-3-319-06540-3_25-3

[36] C.Klingshirn, "Energy transfer in Semiconductors," *Angew. Chemie Int. Ed. 6(11), 285–370,*Volume 114, 1967, doi: 10.1007/978-1-4613-2407-2.

[37] D. C. Look, D. C. Reynolds, C. W. Litton, R. L. Jones, D. B. Eason, and G. Cantwell, "Characterization of homoepitaxial p-type ZnO grown by molecular beam epitaxy," *Appl. Phys. Lett.*, vol. 81, no. 10, pp. 1830–1832, 2002, doi: 10.1063/1.1504875.

[38] K. K. Kim, H. S. Kim, D. K. Hwang, J. H. Lim, and S. J. Park, "Realization of p-type ZnO thin films via phosphorus doping and thermal activation of the dopant," *Appl. Phys. Lett.*, vol. 83, no. 1, pp. 63–65, 2003, doi: 10.1063/1.1591064.

[39] Z. Wang, S. C. Su, M. Younas, F. C. C. Ling, W. Anwand, and A. Wagner, "The Zn-vacancy related green luminescence and donor-acceptor pair emission in ZnO grown by pulsed laser deposition," *RSC Adv.*, vol. 5, no. 17, pp. 12530–12535, 2015, doi: 10.1039/c4ra13084g.

[40] S. L. Shi, G. Q. Li, S. J. Xu, Y. Zhao, and G. H. Chen, "Green luminescence band in ZnO: Fine structures, electron-phonon coupling, and temperature effect," *J. Phys. Chem. B*, vol. 110, no. 21, pp. 10475–10478, 2006, doi: 10.1021/jp0610968.

[41] D. I. Florescu, L. G. Mourokh, F. H. Pollak, D. C. Look, G. Cantwell, and X. Li, "High spatial resolution thermal conductivity of bulk ZnO (0001)," *J. Appl. Phys.*, vol. 91, no. 2, pp. 890–892, 2002, doi: 10.1063/1.1426234.

[42] Ü. Özgür *et al.*, "Thermal conductivity of bulk ZnO after different thermal treatments," *J. Electron. Mater.*, vol. 35, no. 4, pp. 550–555, 2006, doi: 10.1007/s11664-006-0098-9.

[43] L. Zhang, T. Tosho, N. Okinaka, and T. Akiyama, "Thermoelectric properties of solution combustion synthesized Al-doped ZnO," *Mater. Trans.*, vol. 49, no. 12, pp. 2868–2874, 2008, doi: 10.2320/matertrans.MAW200801.

[44] X. Wu, J. Lee, V. Varshney, J. L. Wohlwend, A. K. Roy, and T. Luo, "Thermal Conductivity of Wurtzite Zinc-Oxide from First-Principles Lattice Dynamics - A Comparative Study with Gallium Nitride," *Sci. Rep.*, vol. 6, no. October 2015, pp. 1–10,

2016, doi: 10.1038/srep22504.

[45] A. Paradisi, J. Biscaras, and A. Shukla, “Inducing conductivity in polycrystalline ZnO1-x thin films through space charge doping,” *J. Appl. Phys.*, vol. 122, no. 9, 2017, doi: 10.1063/1.5001127.

[46] W. Göpel and U. Lampe, “Influence of defects on the electronic structure of zinc oxide surfaces,” *Phys. Rev. B*, vol. 22, no. 12, pp. 6447–6462, 1980, doi: 10.1103/PhysRevB.22.6447.

[47] C. Klingshirn, “ZnO: From basics towards applications,” *Phys. Status Solidi Basic Res.*, vol. 244, no. 9, pp. 3027–3073, 2007, doi: 10.1002/pssb.200743072.

[48] S. U. Jen, H. Sun, H. P. Chiang, S. C. Chen, J. Y. Chen, and X. Wang, “Optoelectronic properties and the electrical stability of Ga-doped ZnO thin films prepared via radio frequency sputtering,” *Materials (Basel).*, vol. 9, no. 12, 2016, doi: 10.3390/ma9120987.

[49] J. A. Sans, J. F. Sánchez-Royo, A. Segura, G. Tobias, and E. Canadell, “Chemical effects on the optical band-gap of heavily doped ZnO: MIII (M=Al,Ga,In): An investigation by means of photoelectron spectroscopy, optical measurements under pressure, and band structure calculations,” *Phys. Rev. B - Condens. Matter Mater. Phys.*, vol. 79, no. 19, pp. 1–9, 2009, doi: 10.1103/PhysRevB.79.195105.

[50] J. H. Lim *et al.*, “Synergistic effect of Indium and Gallium co-doping on growth behavior and physical properties of hydrothermally grown ZnO nanorods,” *Sci. Rep.*, vol. 7, no. February, 2017, doi: 10.1038/srep41992.

[51] R. Sankar ganesh *et al.*, “Influence of Al doping on the structural, morphological, optical, and gas sensing properties of ZnO nanorods,” *J. Alloys Compd.*, vol. 698, pp. 555–564, 2017, doi: 10.1016/j.jallcom.2016.12.187.

[52] Z. Gao and P. Banerjee, “Review Article: Atomic layer deposition of doped ZnO films,” *J. Vac. Sci. Technol. A*, vol. 37, no. 5, p. 050802, 2019, doi: 10.1116/1.5112777.

[53] M. Saha, S. Ghosh, V. D. Ashok, and S. K. De, “Carrier concentration dependent optical and electrical properties of Ga doped ZnO hexagonal nanocrystals,” *Phys. Chem. Chem. Phys.*, vol. 17, no. 24, pp. 16067–16079, 2015, doi: 10.1039/c4cp05480f.

[54] A. Abduev, A. Akmedov, A. Asvarov, and A. Chiolerio, “A revised growth model for transparent conducting Ga doped ZnO films: Improving crystallinity by means of buffer layers,” *Plasma Process. Polym.*, vol. 12, no. 8, pp. 725–733, 2015, doi: 10.1002/ppap.201400230.

[55] Z. R. Tian *et al.*, “Complex and oriented ZnO nanostructures,” *Nat. Mater.*, vol. 2, no. 12, pp. 821–826, 2003, doi: 10.1038/nmat1014.

[56] K. G. Harstad and J. Bellan , "Mixing rules for multicomponent mixture mass diffusion coefficients and thermal diffusion factors", J. Chem. Phys. 120, 5664-5673 (2004) https://doi.org/10.1063/1.1650296

[57] N. T. Eldabe, R. R. Rizkalla, M. Y. Abouzeid, and V. M. Ayad, “Thermal diffusion and diffusion thermo effects of Eyring-Powell nanofluid flow with gyrotactic microorganisms through the boundary layer,” *Heat Transf. - Asian Res.*, vol. 49, no. 1, pp. 383–405, 2020, doi: 10.1002/htj.21617.

[58] T. Nakagawa *et al.*, “Diffusion model of gallium in single-crystal zno proposed from analysis of concentration-dependent profiles based on the fermi-level effect,” *Japanese J. Appl. Physics, Part 1 Regul. Pap. Short Notes Rev. Pap.*, vol. 46, no. 7 A, pp. 4099–4101, 2007, doi: 10.1143/JJAP.46.4099.

[59] C. Periasamy, R. Prakash, and P. Chakrabarti, “Effect of post annealing on structural and optical properties of ZnO thin films deposited by vacuum coating technique,” *J. Mater. Sci. Mater. Electron.*, vol. 21, no. 3, pp. 309–315, 2010, doi: 10.1007/s10854-009-9912-5.

[60] Z. Li and W. Gao, “ZnO thin films with DC and RF reactive sputtering,” *Mater. Lett.*, vol. 58, no. 7–8, pp. 1363–1370, 2004, doi: 10.1016/j.matlet.2003.09.028.

[61] J.-C. Hsu and Y.-S. Chiang, “Influence of Oxygen on Zinc Oxide Films Fabricated by Ion-Beam Sputter Deposition,” *ISRN Mater. Sci.*, vol. 2013, pp. 1–7, 2013, doi: 10.1155/2013/710798.

[62] M. Opel, S. Geprägs, M. Althammer, T. Brenninger, and R. Gross, “Laser molecular beam epitaxy of ZnO thin films and heterostructures,” *J. Phys. D. Appl. Phys.*, vol. 47, no. 3, 2014, doi: 10.1088/0022-3727/47/3/034002.

[63] K. Nomura, H. Ohta, K. Ueda, T. Kamiya, M. Hirano, and H. Hosono, “Thin-film transistor fabricated in single-crystalline transparent oxide semiconductor,” *Science (80-.).*, vol. 300, no. 5623, pp. 1269–1272, 2003, doi: 10.1126/science.1083212.

[64] J. J. Huang *et al.*, “Influences of low temperature silicon nitride films on the electrical performances of hydrogenated amorphous silicon thin film transistors,” *J. Phys. D. Appl. Phys.*, vol. 41, no. 24, 2008, doi: 10.1088/0022-3727/41/24/245502.

[65] H. Lee, G. Yoo, J. S. Yoo, and J. Kanicki, “Asymmetric electrical properties of fork a-Si:H thin-film transistor and its application to flat panel displays,” *J. Appl. Phys.*, vol. 105, no. 12, 2009, doi: 10.1063/1.3153968.

[66] N. Kimizuka and T. Mohri, “Spinel, YbFe2O4, and Yb2Fe3O7 types of structures for compounds in the In2O3 and Sc2O3A2O3BO systems [A: Fe, Ga, or Al; B: Mg, Mn, Fe, Ni, Cu, or Zn] at temperatures over 1000°C,” *J. Solid State Chem.*, vol. 60, no. 3, pp. 382–384, 1985, doi: 10.1016/0022-4596(85)90290-7.

[67] K. Nomura, H. Ohta, A. Takagi, T. Kamiya, M. Hirano, and H. Hosono, “Room-temperature fabrication of transparent flexible thin-film transistors using amorphous oxide semiconductors,” *Nature*, vol. 432, no. 7016, pp. 488–492, 2004, doi: 10.1038/nature03090.

[68] C. L. Lin, P. C. Lai, P. C. Lai, P. S. Chen, and W. L. Wu, “Pixel Circuit with Parallel Driving Scheme for Compensating Luminance Variation Based on a-IGZO TFT for AMOLED Displays,” *J. Disp. Technol.*, vol. 12, no. 12, pp. 1681–1687, 2016, doi: 10.1109/JDT.2016.2616507.

[69] T. Arai and T. Sasaoka, “Invited paper: Emergent oxide TFT technologies for next-generation AM-OLED displays,” *49th Annu. SID Symp. Semin. Exhib. 2011, Disp. Week 2011*, vol. 2, pp. 710–713, 2011, doi: 10.1889/1.3621424.

[70] M. Ito, M. Kon, M. Ishizaki, and N. Sekine, “A Flexible Active-matrix TFT Array with Amorphous,” *Idw/Ad’05*, no. August, pp. 845–846, 2005.

[71] H. Jeong *et al.*, “Temperature sensor made of amorphous indium-gallium-zinc oxide TFTs,” *IEEE Electron Device Lett.*, vol. 34, no. 12, pp. 1569–1571, 2013, doi: 10.1109/LED.2013.2286824.

[72] H. Frenzel *et al.*, “ZnO metal-semiconductor field-effect transistors with Ag-Schottky gates,” *Appl. Phys. Lett.*, vol. 92, no. 19, 2008, doi: 10.1063/1.2926684.

[73] P. Görrn *et al.*, “Stability of transparent zinc tin oxide transistors under bias stress,” *Appl. Phys. Lett.*, vol. 90, no. 6, 2007, doi: 10.1063/1.2458457.

[74] J.S Yuan and J.J Liou, Ed., *Semiconductor Device Physics and Simulation*. Menlo park, California: SRI International, 1996.

[75] H. Frenzel, A. Lajn, H. von Wenckstern, G. Biehne, H. Hochmuth, and M. Grundmann, “ZnO-based metal-semiconductor field-effect transistors with Ag-, Pt-, Pd-, and Au-Schottky gates,” *Thin Solid Films*, vol. 518, no. 4, pp. 1119–1123, 2009, doi: 10.1016/j.tsf.2009.02.149.

[76] H. Frenzel *et al.*, “ZnO-based metal-semiconductor field-effect transistors on glass substrates,” *Appl. Phys. Lett.*, vol. 95, no. 15, pp. 18–21, 2009, doi: 10.1063/1.3242414.

[77] “ZnO-based MESFET Devices M. Grundmann, H. Frenzel, A. Lajn, H. von Wenckstern, F. Schein, and M. Lorenz Universität Leipzig, Institut für Experimentelle Physik II, Linnéstr. 5, 04103 Leipzig, Germany,” vol. 1201, no. c, pp. 3–7, 2010.

3. Research Methodology

3.1 NPs layer formation

3.1.1 Fabrication of ZnO NPs

ZnO-NPs were synthesized using the arc-discharge-mediated gas evaporation process. In the arc plasma method[1], as a zinc source, commercially available zinc (4N) rod was employed, and dry air was injected (5 L/min), while a carbon rod acted as a cathode. To form a ϕ 2×2 cm cylindrical Zn metal block, the zinc rod was cut into small pieces of 1 cm range, placed in an aluminum crucible, and heated to 600°C in an ambient atmosphere for an hour[1]. In the arc plasma unit, the Zn block is being positioned on the holder (anode) inside a cylindrical chamber. **Fig. 3.1** depicts the vertical layout of the free burning arc discharge experimental setup. The cathode (carbon rod) was adjusted to a few mm from the anode (Zn block) and the arc current was initiated by dc power supply after controlling the fabrication conditions of current density, chamber pressure, and the flow of dry air. As a result, the breakdown voltage was formed between the tiny gap of cylindrical carbon cathode and a flat zinc anode, resulting in ionized plasmas and collisions of a charged particle[1]. The arc current can be controlled depending on the fabrication condition and it can be produced in a range of 1~100 A.

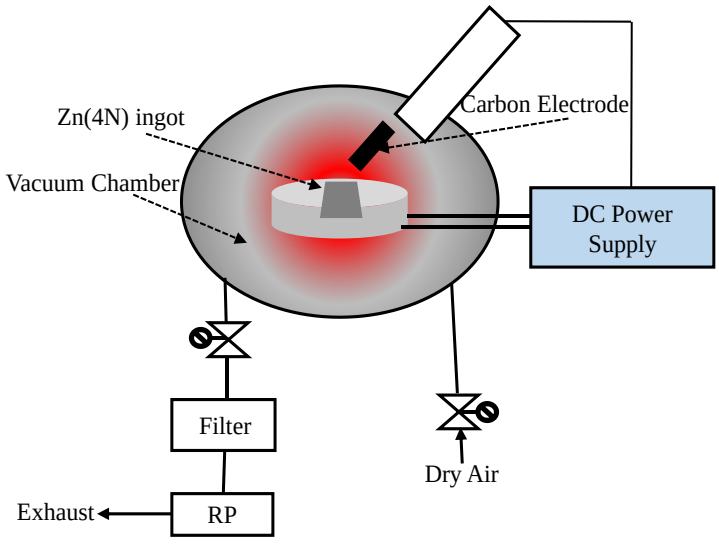

Fig.3.1 Symmetric illustration of the arc-discharge-mediated gas evaporation NPs formation method

The chamber pressure was controlled using a rotary vacuum pump in the range 50~780 Torr. The compressed dry air was injected into the chamber at a rate of 5 L/min, which was regulated by a flow controller. The 610 Torr and the 20 A arc current was used to fabricate the n-type ZnO NPs which is used in this study. In addition, the nitrogen content of the produced ZnO nanoparticles can be changed by controlling the pressure and the discharge current according to the inflow of dry air[2]. **Fig.3.2** shows the changes of nitrogen concentration by controlling the pressure and current during the flow of dry air. ZnO crystals exhibit n-type characteristics due to inherent defects, but since nitrogen acts as an acceptor, they exhibit p-type characteristics when the nitrogen content is high[3].

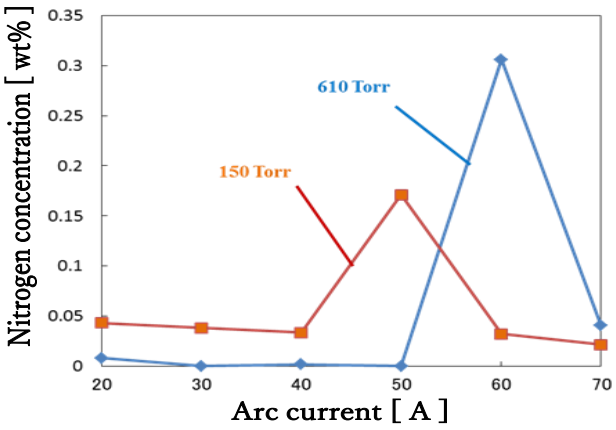

Fig.3.2 N_2 concentration based on the arc current.
Referring [2]

3.1.2 Ga doping into ZnO NPs

Our laboratory synthesized ZnO and Ga_2O_3 particles manufactured by Sigma-Aldrich Co. Ltd. were mixed by vortex and subjected to thermal diffusion treatment. **Fig. 3.3 (a)** shows the electric furnace (manufactured by Fulltech, FT-01VAC-30) which is used for heat treatment. **Fig. 3.3 (b)** shows a simplified annealing furnace. The annealing process is carried out into several atmospheric conditions like open-air, dry nitrogen (N_2), dry oxygen (O_2), wet-air, and dry-air only under temperatures ranging from 600~900°C for 60min. The open-air contains both N_2 and O_2 content and is performed under high humidity conditions.

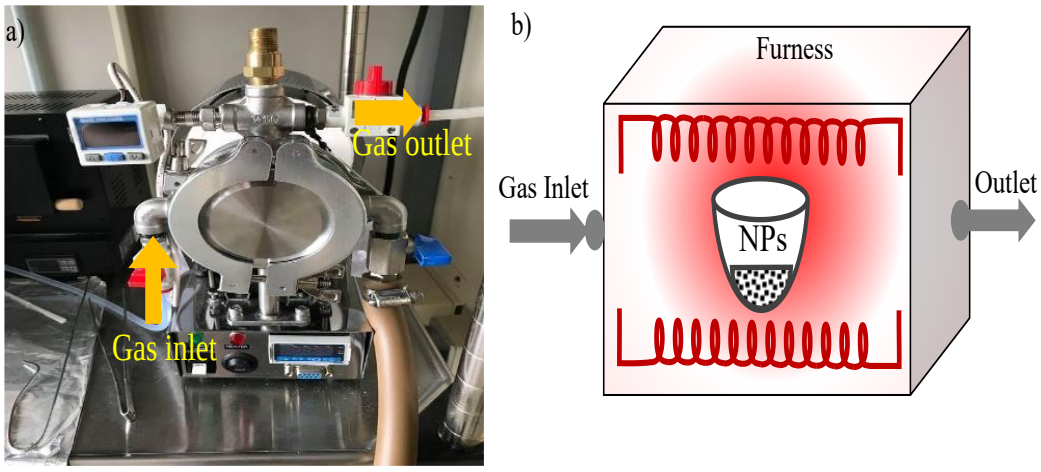

Fig.3.3 (a) Electrical furnace 3(b) illustration of the simplified annealing furnace

3.1.3 Dispersion processing

The above annealed ZnO NPs dispersing by Ultrasonics homogenizer with 10g of ultrapure water. After dispersing the Centrifugal separator was used to separate the large particles from the solution. By using this most of the residual Ga_2O_3 was removed resulting in the 100 to 150nm median size NPs. **Table 1 & 2** shows the detailed conditions for dispersion processing.

Table1. Ultrasonic homogenizer condition

Time[min]	Power%[W]	Pulse on/off time[sec]
3	150	5

Table2. Centrifugal separator condition

Rotating Speed[G]	Time[min]
3000	1

3.1.4 NPs layer fabrication:

The above dispersed 10 ml dispersion was sprayed onto the heated quartz substrate. In this method, sintering of the particles takes time and agglomerates, and it is manufactured by a spray-coating technic using an airbrush as shown in **Fig. 3.4**. The general spraying method may be carried out in atmospheric gas or reduced atmosphere pressure, but in this study, it is carried out under atmospheric pressure. First by increasing the temperature of the hot plate by keeping the amount to be sprayed constant, the sprayed ZnO nanoparticle dispersion to form a nanoparticle layer by adjusting the temperature of the hot plate. At this time, though it is thought that suppression of the amount of evaporation of nitrogen can be achieved. However, if the distance between the airbrush injection port and the substrate is small, more particles can be attached to the substrate, but the particles tend to aggregate readily if the distance is larger, resulting in a gap in the layer. The 7ml of dispersion fluid was sprayed to the heated quartz substrate under the condition of **table 3**. The thickness can be controlled by varying the centrifuge condition at the time of dispersion processing. On the time of sparing the dispersion sprayed onto the heated quartz substrate with the hot plate temperature of 500°C but the thermographic measurements stated that the surface temperature is around 370°C during spraying. The 5s interval was used from one to another shot of spray causing the surface temperature drastically to decrease after dropped the dispersion onto the substrate and it goes back to the previous state during that interval. By taking the intervals during spraying the uniformity of the sprayed layer can be unchanged.

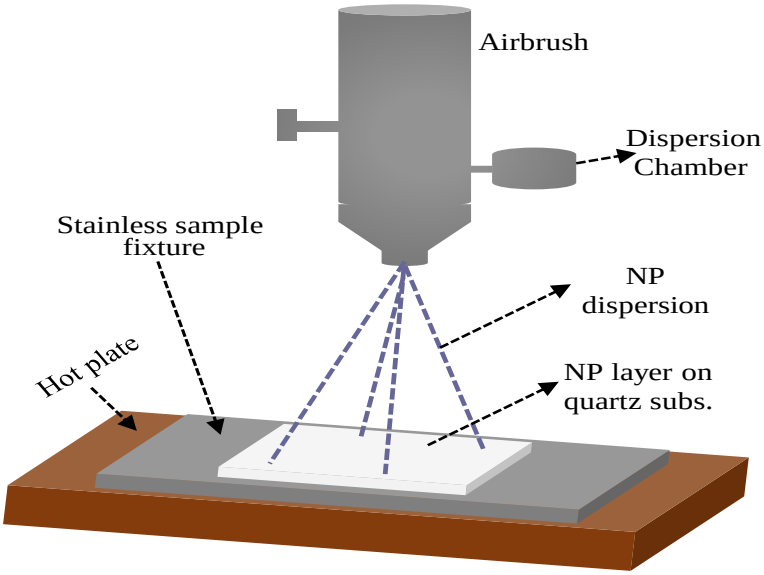

Fig.3.4 Illustration of the spray coating process for NPs layer fabrication

Table 3 Sprayed layer formation condition:

Dispersion[ml]	~7
Distance (from injection point to substrate) [cm]	15
Spray interval [sec]	5
Hot plate temperature [℃]	500

3.2 MESFET fabrication

The operation of MESFET (Metal Semiconductor-Field Effect Transistor) is similar to that of a junction field-effect transistor (JFET)[4]. MESFET does not use the oxide film (insulating film) used in general transistors such as MOSFET[5]. In addition, it is a unipolar device with one type of carrier conduction, and in addition, it uses Schottky

characteristics that use a potential barrier when a metal and a semiconductor come into contact with each other. N-type III-V compound semiconductors are used for MESFETs fabrication because of their high electron mobilities and average drift velocities. A schematic illustration of the MESFET device is shown in **Fig. 3.5**. The ZnO TFTs used in this study were top-gate depletion-mode MESFET devices. The n-type ZnO channel layer (~1 μm) was grown on a glass substrate by spray coating, and Al evaporation (~50 nm) was used as the source (S) and drain (D) ohmic contacts. Finally, a gold (Au) Schottky gate electrode was fabricated between the S and D contacts using a sputter (~30 nm).

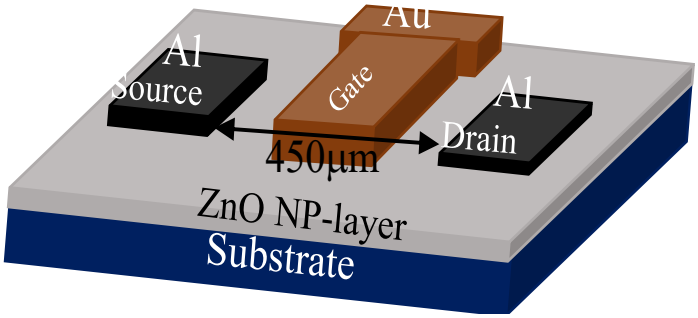

Fig.3.5 Symmetric illustration of MESFET structure

3.3 Experimental techniques

3.3.1 Current-Voltage (*I-V*) measurement

In order to measure the *I-V* characteristics in a thin film, three methods are being used. The two-probe, four-probe, and three-probe *I-V* measurement methods are the three common methods. The term "two-probe measurement" refers to two wires that are physically attached to the two electrodes of the practical device. Two independent contact pairings are used in the four-probe measurement, one for applying the calibrated current and the other for measuring the voltage. In a three-probe measurement, between the two electrodes, a third microelectrode is used. The advantage of using a four-point probe

measurement is that the contact contribution can be eliminated. The most frequent measurement method is the two-point probe measurement, which is simple to set up.

In our present work, the evaluation of the ZnO NPs layer is carried out by a two-point probe *I-V* characteristic measuring apparatus**.** This is the simplest method of measuring resistivity. A symmetric illustration of *I-V* measurement shows in **Fig.3.6.** The resistivity can be measured using equation (1).

$$\rho = \frac{\Delta V}{\Delta I} \quad \text{..... (1)}$$

Where: ρ is the resistivity.

Light is shielded by placing a sample in the shield box and the two probes are brought into contact with Au electrodes to evaluate conductivity. Sets the voltage value range to -10 V to 10 V.

In my samples 0.3mm x 0.3mm square shape electrodes were used, so the sheet resistance can be directly obtained from the slope of *I-V* curves. So, the Sheet resistance is given by the equation (2).

$$Rs = R.\frac{W}{L} \quad \text{..... (2)}$$

Where: R_s is the sheet resistance; R is the measured resistivity of the samples; W is the width of the electrodes; L is the length between the electrodes.

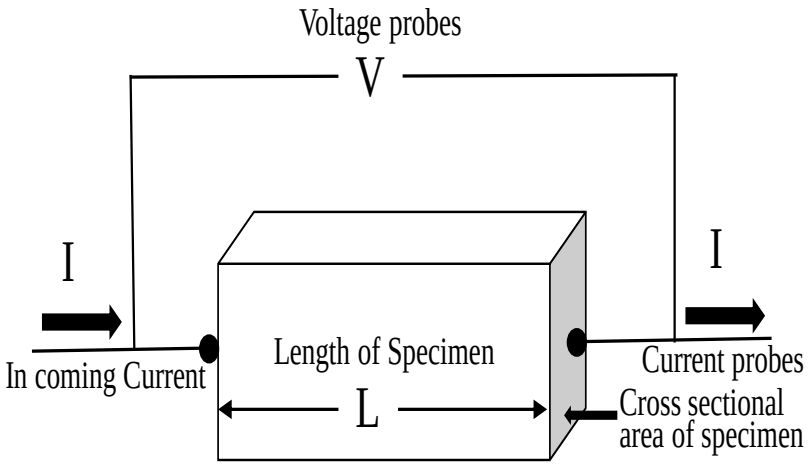

Fig.3.6 A symmetric illustration of *I-V* measurement

3.3.2 Optical measurement: Photoluminescence (PL)

Photoluminescence spectroscopy (PL spectroscopy) is a useful method for investigating semiconductor properties and identifying native point defects. The light from the source is directed onto a sample, where it is absorbed and photoexcitation might occur, resulting in the emission of PL. The approach can reveal information on semiconductors' photochemical and optical properties, as well as their electronic structure and point defects in the interfacial region. Since this luminescence is easily affected by impurities and defects in the substance, it is possible to obtain information on the presence, type, and defects of impurities in the substance by spectroscopically analyzing the luminescence. In addition, PL measurement is generally non-destructive measurement and does not require pretreatment. A symmetric illustration of PL measurement is shown in **fig. 3.7.**

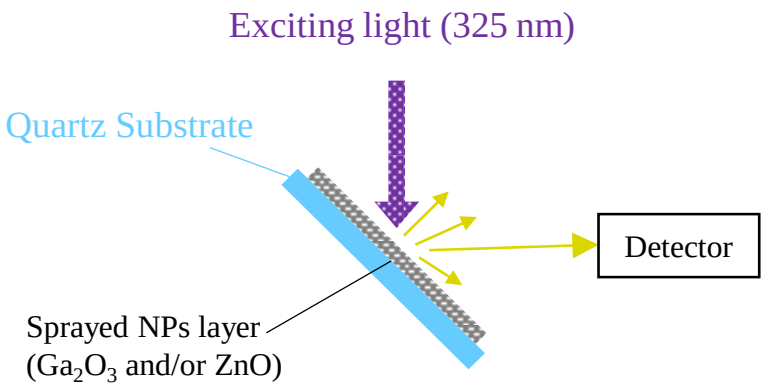

Fig.3.7 Symmetric illustration of PL measurement

In this study, the optical properties of sprayed NP layers were measured by a Fluromax-4 spectrofluorometer in the wavelength range from 340~600 nm.It is possible to identify material defects and impurities by analyzing the luminescence spectrum. The light scattered from inside a crystal and the method captured the defects. This approach can easily obtain a defect signal if a crystal has a low carrier concentration. In our measurement system spray-coated ZnO NPs layer with quartz substrate placed in 30 or 60-degree angle for front and back PL measurement respectively. The PL spectra of ZnO grown at room temperature with various sprayed samples consist of an excitation wavelength of 325 nm with 0.2 s exposure time. The exciton/defect ratio grew at 340nm to 600nm wavelength visible region.

3.3.3 Structural Measurements: X-Ray Diffraction (XRD)

X-ray diffraction is a nondestructive technique for analyzing thin films. It can be used to calculate the lattice parameter value, identify phases, and determine crystallographic orientation and texture. A material is examined with x-rays with wavelengths near to lattice spacing in x-ray diffraction. Bragg's law[6] specifies the conditions for diffraction.

$$n\lambda = 2dsin\theta \ldots\ldots\ldots\ldots \quad (3)$$

In this study, 2θ scans from 15° to 80° with sampling step of 0.02° were performed by SmartLab, Rigaku Corporation, λ=1.54 Å diffractometer and Cu-Kα radiation. The sample can be rotated along with one of the axes (θ-axis) and the detector can be rotated

independently (2θ-axis) in this two-circle diffractometer. **Fig.3.8** shows a schematic diagram of the diffractometer.

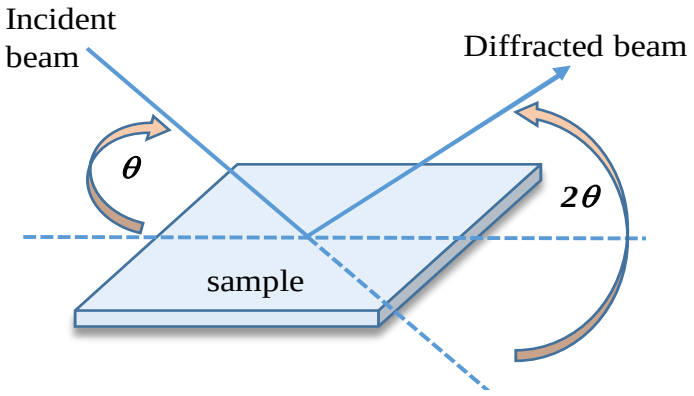

Fig.3.8 Schematic diagram of the diffractometer.

The Bragg-Brentano diffraction geometry is used in this diffractometer. In this geometry, the diffracted beam is often in the plane containing both the incident and normal beams. This diffractometer can only acquire diffraction data from surfaces that is parallel to the sample's face since the sample can only be oriented along the -axis. A four-circle diffractometer can be used to determine the film/layers in-plane orientation. In this setup, the specimen can be rotated in response to the incident beam and rotate at 360 degrees all around surface. The most common method for characterization of thin films/layers is 2θ diffraction measurement. The lattice constant of *a*-axis and *c*-axis are calculated from *101* and *002* peak positions using 2θ measurement also the crystallite size was calculated using Scherrer's formula [7].

$$\frac{1}{d^2_{hkl}} = [\frac{4}{3}(h^2+k^2+hk)+l^2(\frac{a}{c})^2]\frac{1}{a^2} \text{.....(4)}$$

where d_{hkl} is the interplanar spacing calculated from Bragg's equation, and *h*, *k*, and *l* are the Miller indices.

3.3.4 X-Ray Photoelectron Spectroscopy (XPS)

When the surface of a sample is irradiated with X-rays under vacuum, photoelectrons

are emitted into the vacuum from the surface (photoelectric effect). A symmetric illustration of XPS measurement is shown in **Fig. 3.9.**

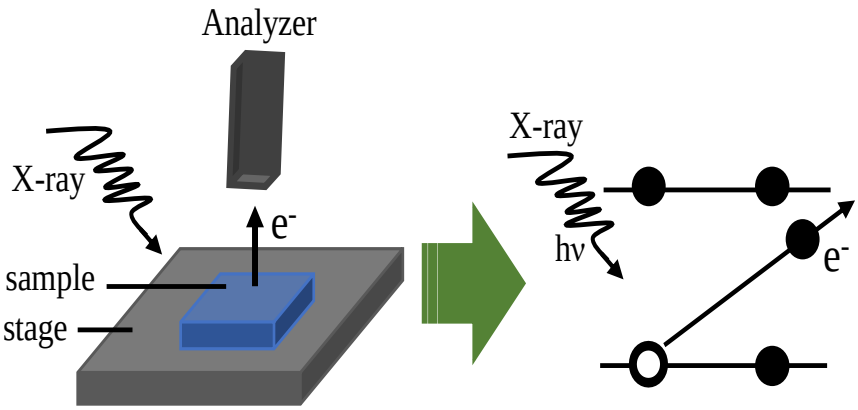

Fig.3.9 symmetric illustration of XPS measurement

The kinetic energy of the photoelectrons can be measured to obtain information on the elements and chemical states of the sample surface and the relationship formula[8] shown in equation (5).

$$EB = h_v - KE \quad \ldots\ldots\ldots\ldots (5)$$

E_b is the binding energy of bound electrons, h_v is the energy of irradiated X-rays, and E_k is the kinetic energy of photoelectrons. Since the binding energy of bound electrons is unique to the element, the element existing on the surface of the substance can be determined by analyzing the energy spectrum of the photoelectron. In addition, since the peak position of each element shifts slightly due to the difference in the chemical state of the surface, information on the valence band state can be obtained from the shift. Since the distance (mean free path) that photoelectrons travel in a substance without inelastic scattering is several nm, the detection depth in this analysis method is several nm. XPS can measure insulation samples relatively easily and can also analyze in the depth direction. For use in this research, we asked the Research Center for Quantum Integrated Electronics, Hokkaido University to measure the sample.

3.3.5 Dynamic Light scattering (DLS) measurement

To know the particle size of the NPs Dynamic Light scattering (DLS) particle size analyzer was used. DLS is a well-established non-invasive technology for determining particle size and size distribution. Particle size can be calculated by measuring the random variations in the intensity of light scattered from a suspension or solution caused by the Brownian motion (random thermal motion) of the small particles in suspension. The laser light is dispersed at varying intensities due to Brownian motion of particles or molecules in suspension. Using the Stokes-Einstein equation, the velocity of Brownian motion and thus the particle size may be calculated from these intensity fluctuations[9].

$$D_h = \frac{k_B T}{3\pi\eta D_t} \quad \ldots\ldots\ldots\ldots\ldots (6)$$

Where D_h is the hydrodynamic diameter D_t is the translational diffusion, k_B is Boltzmann's constant, T is thermodynamic temperature, η is the dynamic viscosity.

For measuring the particle size of ZnO and Ga_2O_3 nanoparticles, (HORIBA, LB-550VS) was used. The symmetric illustration of DLS measurement is shown in **Fig. 3.10**. Nanoparticles were dispersed in pure water for the experiment and the particle size distribution was recorded.

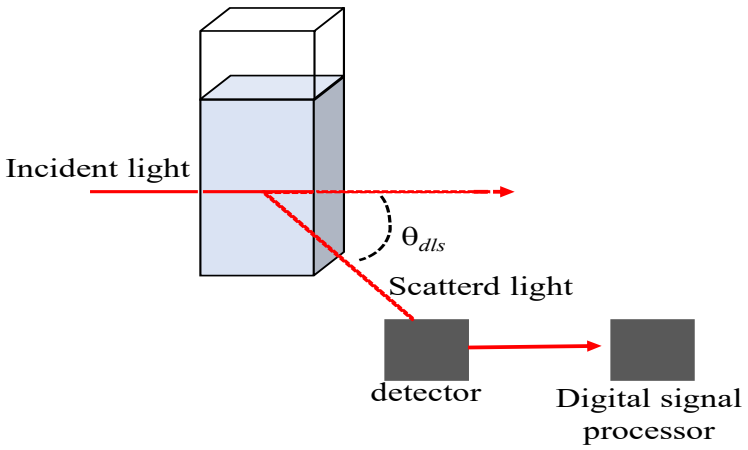

Fig.3.10 symmetric illustration of DLS measurement

3.3.6 UV-Vis Spectroscopy

Spectroscopic measurement is a method of evaluating how much light is emitted (how much light is absorbed by a sample) with respect to the light emitted to the sample. At this time, the intensity I_0 of the incident light and the intensity I of the transmitted light generally have a relationship called Lambert-Beer's law[10].

$$I = I_0 e^{-kt} \quad \ldots\ldots\ldots\ldots\ldots\ldots (7)$$

Where I = Intensity of light after passing through the samples,

I_0 = Intensity of light before passing through the samples, and

K = absorbance of 1cm pathlength samples.

Transmittance is related to the intensity of light after it passes through the cuvette (T). The fraction of light that passes through the sample is known as transmittance. The equation can be used to determine the transmittance.

$$T = \frac{I}{I_0} \quad \ldots\ldots\ldots\ldots\ldots\ldots\ldots (8)$$

Transmittance is related to absorption (A) and can be stated by the following equation[8].

$$A = -\log(T) = -\log \frac{I}{I_0} \quad \ldots\ldots\ldots (9)$$

A UV-Vis spectrophotometer compares the light intensity passing through a sample (I) vs. light intensity before it passes through (I_0), represented as absorbance (A) or transmittance (T). The spectrophotometer uses a tungsten source to produce visible and near-infrared radiation and is a double beam double monochromator type. The beam is separated into two sections, one of which is directed at the ZnO sample and the other of which goes through a blank control area (substrate). The route lengths of the split beams are all the same. After that, the detector compares the intensity of the two beams and estimates the film's transmittance in relation to the substrate. The equipment compensates for beam variations since the sample and reference beams are compared simultaneously. The optical transmittance spectrum of ZnO thin film was obtained using UV-Vis spectroscopic measurement in the wavelength range of 200 to 1100 nm. The absorption coefficient, band gap energy, Refractive index, extinction coefficient, and Urban energy can be determined using the measured spectrum[11].

Shimadzu UV-Vis Spectrophotometer was used for the measurements. The symmetric illustration of this measurement is shown in **Fig. 3.11**.

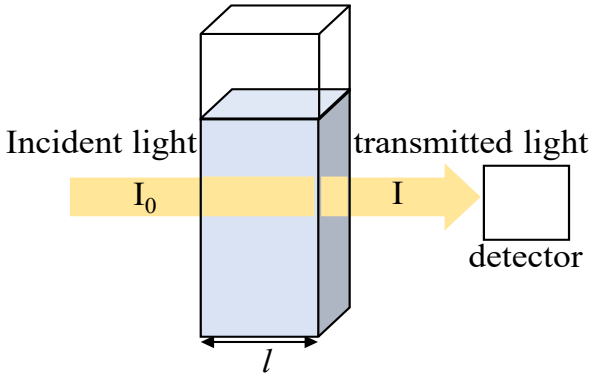

Fig.3.11 Symmetric illustration of UV-VIS Spectroscopy measurement

3.4 References

[1] K. Senthilkumar, O. Senthilkumar, S. Morito, T. Ohba, and Y. Fujita, "Synthesis of zinc oxide nanoparticles by dc arc dusty plasma," *J. Nanoparticle Res.*, vol. 14, no. 10, 2012, doi: 10.1007/s11051-012-1205-x.

[2]. Itohara Daiki, "Formation of ZnO nano particle layers by spray method and device application", Masters thesis (2016), Shimane University, Shimane, Japan (written in Japanese, not disclosed).

[3] Y. Fujita, K. Moriyama, Y. Hiragino, Y. Furubayashi, H. Hashimoto, and T. Yoshida, "Electroluminescence from nitrogen doped ZnO nanoparticles," *Phys. Status Solidi Curr. Top. Solid State Phys.*, vol. 11, no. 7–8, pp. 1260–1262, 2014, doi: 10.1002/pssc.201300645.

[4] "ZnO-based MESFET Devices M. Grundmann, H. Frenzel, A. Lajn, H. von Wenckstern, F. Schein, and M. Lorenz Universität Leipzig, Institut für Experimentelle Physik II, Linnéstr. 5, 04103 Leipzig, Germany," vol. 1201, no. c, pp. 3–7, 2010.

[5] M. F. M. Fathil *et al.*, "Deposition and characterization of ZnO thin film for FET with back gate biasing-based biosensors application," *RSM 2015 - 2015 IEEE Reg. Symp. Micro*

Nano Electron. Proc., pp. 1–4, 2015, doi: 10.1109/RSM.2015.7355033.

[6] S. R. S. B.D. Cullity, *Elements of X-ray Diffraction, Third Edition*. New York: Prentice-Hall, 2001.

[7] J. L. Tian, G. G. Wang, and H. Y. Zhang, "Effect of annealing atmosphere on the structural and optical properties of ZnO thin films on Si (100) substrates grown by atomic layer deposition," *J. Nano Res.*, vol. 37, pp. 92–98, 2016, doi: 10.4028/www.scientific.net/JNanoR.37.92.

[8] https://chem.libretexts.org/Bookshelves/Physical_and_Theoretical_Chemistry_Textbook_Maps/Book%3A_Surface_Science_(Nix)/05%3A_Surface_Analytical_Techniques/5.03%3A_Photoelectron_Spectroscopy

[9] https://www.horiba.com/sgp/en-en/technology/measurement-and-control-techniques/material-characterization/dynamic-light-scattering/

[10] http://life.nthu.edu.tw/~labcjw/BioPhyChem/Spectroscopy/beerslaw.htm

[11] RASHEED, Mohammed & Barille, Regis. (2017). Room Temperature deposition of ZnO and Al:ZnO ultrathin films on glass and PET substrates by DC sputtering Technique. Optical and Quantum Electronics. 49. 10.1007/s11082-017-1030-7.

4. Ga-Doping into ZnO Nanoparticles using Thermal Diffusion Process

4.1 Introduction

To obtain the conductive channel layer of thin-film transistors (TFTs), the semiconductor nanoparticle (NP) layer is one of the notable methods[1]–[5] because of its high selectivity of substrate materials, surface morphology, its compatibility of the printing electronics, atmospheric processing, the low costing, and the large area process and so on. Controlling the electrical conductivity of ZnO has remained a significant concern despite recent rapid advances. Therefore, many efforts have been made to form and demonstrate TFTs with the n-type ZnO-NP channels on various substrates[1], [6]–[10] including demonstration of the logic operations[11]. Although a majority of research groups had reported achieving p-type ZnO, there are still concerns about the results' reproducibility and the p-type conductivity's stability. Our group had tried to fabricate both n-channel and p-channel back-gate TFTs on Si/SiO_2 substrates by using the simple and easy spray-coating method using the ZnO-NPs synthesized in our laboratory[12] [13], where NP-layers prepared by ZnO have a high probability of realizing complementary logic circuits. However, the performances of obtained TFTs were degraded due to the extremely high resistivity of horizontal carrier transportation in the sprayed ZnO-NP layers (order of GΩ/sq). Such large parasitic resistances cause the significant degradation of the gain and switching speed in analog and digital operations, respectively. By simple estimation with assuming the logic gate capacitances of several pF, even 100 Hz logic operation will be impossible using these TFTs. Based on the above circumstances, we are concerned to reduce the sheet resistances of obtained ZnO-NP layers for TFT channel applications by impurity doping. The resistivity of impurity-doped ZnO is lower than that of undoped ZnO and it is more stable. Al, Ga, In, B, Si, Ge, Ti, Zr, Hf, and F have previously been doped in ZnO[14] [15]. Ga appears to be the most effective and potential dopant, owing to benefits such as its ionic and covalent radii (0.62 Å and 1.26 Å), which are similar to those of Zn (0.74 and 1.34 Å), resulting in minimal ZnO lattice deformations even at high Ga concentrations[9]. Thermal diffusion and ion planting are the most common method for impurity doping. Direct doping into NPs through the thermal

diffusion process is preferable rather than doping onto the NP-layers, because such doping processes after NP-layer formation should disturb the simplicity of the particle-base process and the selectivity of substrate materials. In this study, the trial of direct Ga-doping into ZnO-NPs by thermal treatment using Ga_2O_3-NPs, confirmation of Ga-diffusion, and the temperature dependence sheet resistance behavior were examined.

This chapter's major content has already been published in the Journal of Surface Science and Nanotechnology as listed on the page of Publications. (T. Yoshida, I. M. Maruful, and Y. Fujita, "Trial of Ga-doping on ZnO nanoparticles by thermal treatment with Ga_2O_3 nanoparticles," *e-Journal Surf. Sci. Nanotechnol.*, vol. 18, pp. 12–17, 2020, doi: 10.1380/EJSSNT.2020.12*).*

4.2 Experimental

ZnO-NPs were synthesized by arc-discharge-mediated gas evaporation method[13], [16]. The detailed NP synthesis process is described in chapter 2 with Refs. 13 and 16, in which n-type conductive particle was recommended. Thus, the conditions to obtain ZnO particles with less nitrogen doping were used. Thermal treatments were applied to some of the obtained ZnO nanoparticles with Ga_2O_3 particles (Sigma-Aldrich Co. Ltd). Particles of ZnO (0.2 g) and Ga_2O_3 (0.06 g) were mixed in the crucible and heated in the electric furnace with a temperature of 600−900°C for 60 min. In this study, two types of ambient gas were applied; one was the atmospheric air which was similar to the gas in NP-synthesizing, and the other was pure nitrogen which would expectedly generate the oxygen vacancies acting as native donors. In thermal treatment with the atmospheric air, the valve of the furnace was opened to the atmosphere and the fresh air (with humidity of about 60%) was supplied by thermal convection. In the case of pure nitrogen, the nitrogen gas with the dew point of less than −60°C and the purity of 99.995% was supplied with the rate of 0.5 L/min. In both cases, the temperature was increased from RT to the setting value within 10 min and after 60 min thermal treatment, the samples were cooled down to less than 40°C in 2 h. The dispersions were prepared by dispersing 0.2 g of above mixed and thermally treated particles with 10 g of ultrapure water using ultrasonic homogenizer with the power of 150 W for 3 min and by following centrifuging with 3000

G for 1 min. To form particle layers[16], 30 mL of dispersion fluid were sprayed to heated quartz substrates using a standard airbrush, as shown in **Fig. 3.4**, with 5-s intervals for 15 min. The setting value of the hot plate temperature was 500°C (the actual surface temperature was about 370°C determined using thermographic measurement). The estimated thickness of particle layers was about 10 μm. Additional Al/Au electrodes with the width and length of 0.3 mm were formed for $I-V$ measurements. $I-V$ measurements to determine the variation of sheet resistances were performed using a shielding prover system and E5270B Precision measurement mainframe with E5287A Atto-level High-Resolution SMU module (Keysight Technologies). Powder X-ray diffraction (XRD) (SmartLab, Rigaku Corporation, $\lambda = 1.54$ Å) was used for 2θ-scan with a scanning speed of 0.001°/step. Elemental analyses were performed by X-ray photoelectron spectroscopy (XPS) with monochromatic Al Kα radiation. The measurements were carried out on the surface of as-sprayed NP-layers without an additional cleaning process. Binding energies were calibrated by shifting the C 1s peak position to 285.0 eV[17], [18].

4.3 Results and discussion

4.3.1 NPs size distribution

The particle size distributions of laboratory synthesized ZnO NPs and Ga_2O_3 NPs are shown in **Fig. 4.1 (a)**, which were prepared by dispersing each particle in ultrapure water by ultrasonic homogenizer without centrifugal separation procedure. ZnO particles that were synthesized in our laboratory have a main peak at around 150 nm and tail distribution over 1000 nm. On the other hand, the Ga_2O_3 particles have sharp distribution with a median size of 667 nm. To confirm the annealing effect of mixed ZnO/Ga_2O_3 NPs with centrifugal separation procedure, the particle size was measured and shown in **Fig. 4.1 (b)**. The particle distribution curve shows sharp distribution with a median diameter of 153 nm. This result helps to reveal that the contribution of large NPs onto the layer can be controlled by the centrifugal separation process. The rest of the dispersion fluid with only a small size of NPs sprayed on the substrate resultant the suppress aggregation phenomenon which was clearly shown in surface properties.

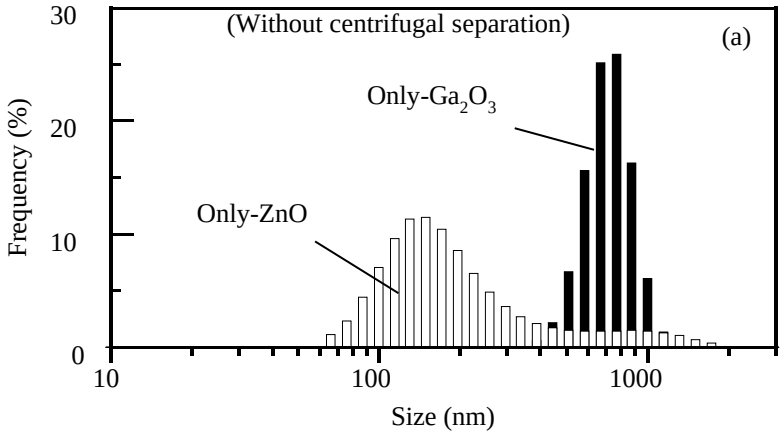

Fig. 4.1 (a) Particle size distributions for separately measured ZnO and Ga_2O_3 NPs without centrifugal separation. Referring [19].

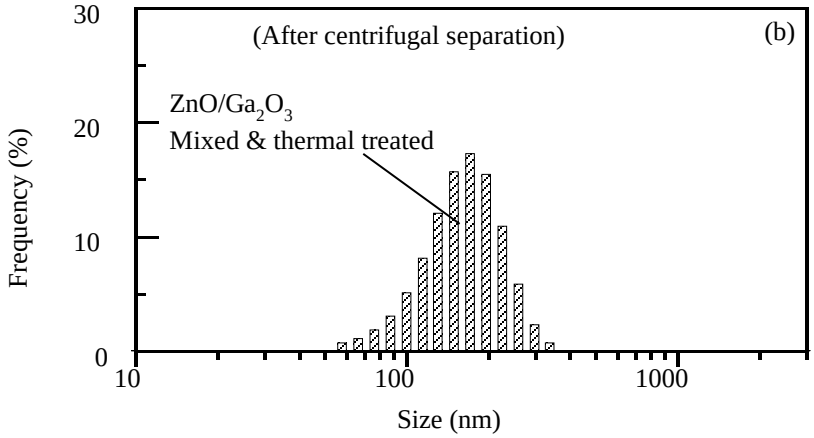

Fig. 4.1 (b) Particle size distributions for mixed and thermally treated ZnO and Ga_2O_3 NPs after centrifugal separation. Referring [19].

4.3.2 Electrical properties

Two probe *I-V* measurement was used with the voltage ranging from -10 V to +10 V and the sheet resistance variations of the fabricated particle layers were studied. The variation of sheet resistance is summarized in **Fig. 4.2**, in which were the 300 μm x 300 μm square shape electrode mask was used, so the sheet resistance can be directly obtained from the slope of *I-V* curves. The measurement was carried out in several points in a sample and Fig indicates the average value obtained from all points. The sprayed particle

layers formed using as-prepared ZnO particles and only mixed with Ga_2O_3 particles (without thermal treatment) show very high sheet resistance in the order of GΩ/sq. These data are labeled "Only ZnO" and "ZnO/Ga_2O_3 only mixed", respectively, and are shown with filled triangles (▲) in **Fig. 4.2**. Circular marks indicate the sheet resistance values for the samples using thermally treated particles; filled circles (●) indicate that the thermal treatments were carried out in atmospheric air and open circles (○) in pure nitrogen. The result revealed that the temperature of thermal treatment less than 700°C had no effect to reduce the sheet resistance[19], which means no impurity doping effects into ZnO particles. On the other hand, thermal treatment with the temperature of 800°C and 900°C showed a significant reduction of 4 to 7 orders of magnitude, especially in atmospheric air annealed at 800°C, which indicate the most impurity doping was achieved in this certain temperature and the minimum value was reached of 225 Ω/sq. As for the confirmation of Ga-doping effect, the sheet resistance was also obtained using thermally treated ‘‘only ZnO’’ particles layer (at 800°C) and indicated in **Fig. 4.2.** The result revealed that no significant effect has been seen in the sheet resistance behavior. Thus, it is confirmed that the property of ZnO particles had been influenced by mixing with Ga_2O_3 particles and thermally treating with the temperature over 800°C. The NPs

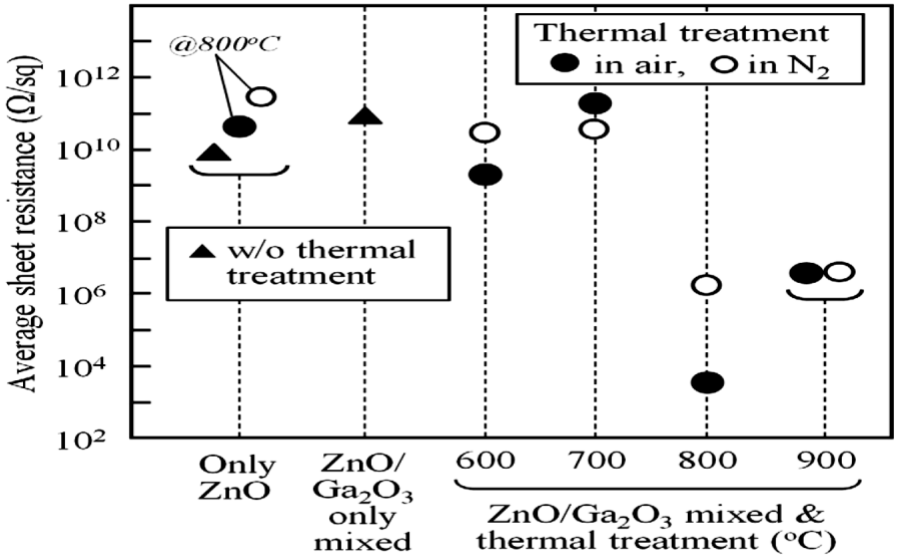

Fig. 4.2 Sheet resistance variations of various kind of particle layers used in this study measured by two-probe I-V measurements. Referring [19].

annealed in the ambient N_2 showed no significant improvement compared with

atmospheric air. The effect of ambient N_2 is clearly shown in chapter 5.

4.3.3 Structural Properties

The structural properties of ZnO nanoparticles (particulates) and NP-layers sprayed with ZnO/Ga_2O_3 mixed and thermally treated (800°C) particles in the air and N_2 are evaluated by XRD measurement, and the result showed in **Fig. 4.3**. Generally known peaks of the ZnO particles with single crystalline state[20,21] were obtained from **Fig. 4.3 (a)**. The result indicates that the undoped ZnO has a preferred orientation of *a*-axis (*100*) and *c*-

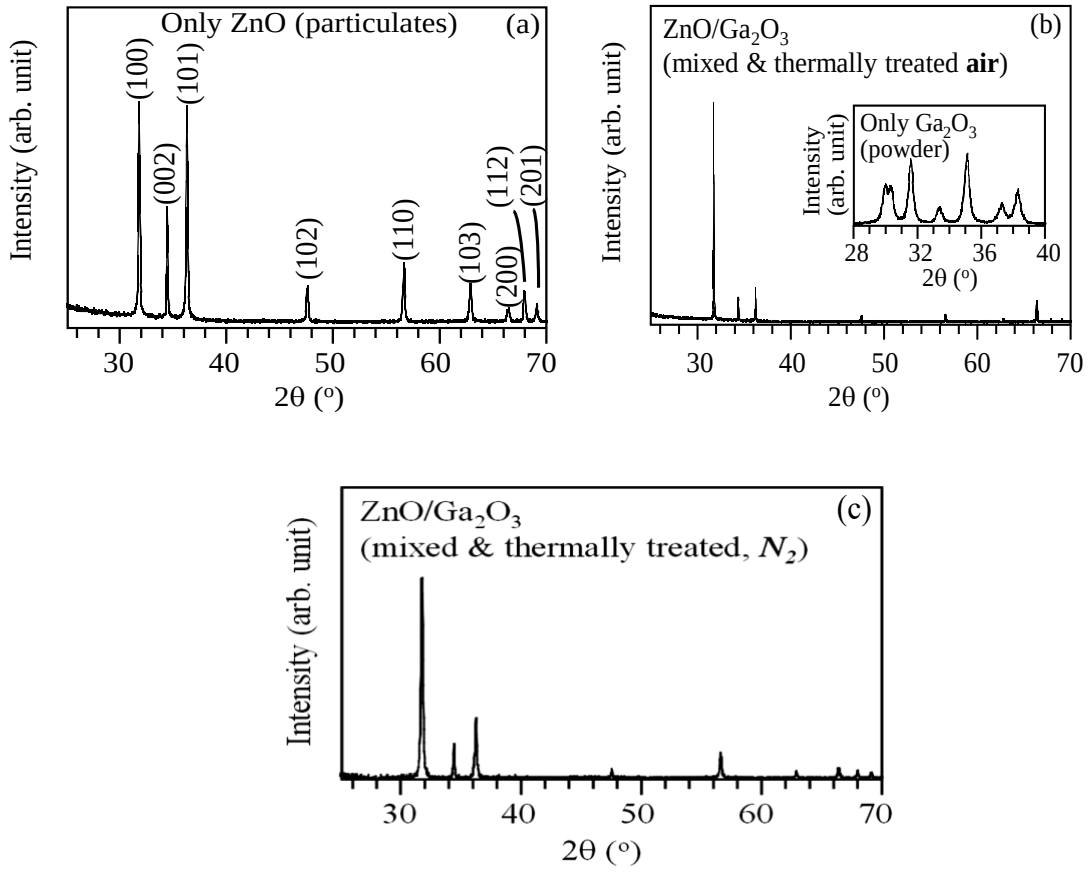

Fig. 4.3 XRD results for (a) ZnO nanoparticles (particulates) and (b and c) NP-layers on quartz substrates sprayed with ZnO/Ga_2O_3 mixed and thermally treated (800°C) particles in air and N_2, respectively. For (b and c), dispersion was prepared with centrifugal separation process. The inset in (b) shows the XRD spectra for Ga_2O_3 particles (particulates). Referring [19].

axis (*002*) both are perpendicular to the substrate. After doping the (*100*) increased (for

both air and N_2 atmosphere) sharply which indicates that the doped ZnO has a preferred orientation of *a*-axis only perpendicular to the substrate. In Fig 4(a, b), full-width at half-maximum (FWHM) values were changed from 0.20° to 0.08° for the (100) peaks by thermal treatment in the air. The crystallite size was calculated using Scherrer's equation and found the improved crystallite size for doped ZnO, especially in the air atmosphere. The calculated crystallite size of ZnO/Ga_2O_3 mixed and thermally treated (800°C) particles in air and N_2 is 100 nm and 45 nm respectively. On the other hand, the XRD spectra of Ga_2O_3 particles used in this study are shown in the inset of **Fig. 4.3(b)**. These peaks are consistent with previous results of the β-Ga_2O_3 particles[22]. But there were no Ga_2O_3-related peaks in **Fig. 4.3(b, c).** It is confirmed, again, that almost all of the residual Ga_2O_3 particles were removed by the centrifugal separation process.

4.3.4 Chemical analysis

To discuss the sheet resistance reduction mechanism, XPS spectra were analyzed. **Fig. 4.4(a)** shows Ga3d spectra for sprayed particle layers made of ZnO/Ga_2O_3 mixed with and without centrifugal separation process (no thermal treatment), ZnO/Ga_2O_3 mixed and thermally treated at 800°C in the air, N_2 with centrifugal separation as a reference, and only ZnO. Overlapping O2s spectra are also shown. The peak intensities were normalized with those of the Zn3d spectra, as shown in the inset of **Fig. 4.4(a)** and the peak positions were shifted to adjust Zn3d at 10.0 eV. The horizontal axis indicates the energy difference from the Zn3d peak where the shifts of energy positions were within ±0.1 eV. The Ga3d spectrum obtained from ZnO/Ga_2O_3 mixed without centrifugal separation shows the largest in-tensity because all Ga_2O_3 particles remained, but after centrifugal separation, only the slight Ga3d component was observed. This again indicates the residual Ga_2O_3 particles can be removed by the suitable centrifugal separation process throughout this study. On the other hand, a relatively large Ga3d peak was observed from ZnO/Ga_2O_3 mixed and thermally treated (800°C) both in the air and N_2 despite being processed with centrifugal separation. These findings strongly suggest that Ga atoms diffused from Ga_2O_3 into the ZnO particles in the thermal treatment process at 800°C. Further analysis on O1s spectra was carried out as shown in **Fig. 4.4(b)**. In this figure, (A) ZnO/Ga_2O_3

and (B) only ZnO particles with thermal treatment (800°C, air) and centrifugal separation were compared. In both samples, the condition difference is only the existence of Ga_2O_3 particles in the thermal treatment process, and they were removed by following centrifugal separation. Considering the fact that the difference between the O1s spectra of O-Zn and O-Ga is 0.8 eV which can be determined using the O1s spectrum of Ga_2O_3 shown in **Fig. 4.4(b)** as a reference. The difference "(A)−(B)" indicates the new component caused by the Ga incorporation into ZnO-NPs. Using the molecular weights of ZnO, Ga_2O_3, and the intensity ratios of the Ga3d or O1s spectrum, the estimated Ga amount in NP-layer of "ZnO/Ga_2O_3 mixed and thermally treated at 800°C in air" is about 5−7 at% assuming a uniform Ga distribution. If this estimate is correct, the measured resistance in **Fig. 4.2** should be one or two orders of magnitude smaller. The reason why so much Ga was detected in **Fig. 4.4** can be considered that diffused Ga was mainly distributed near the surface of the ZnO particles, increasing the effective irradiated area by X-ray and emphasizing the apparent intensity of the Ga3d and Ga-related O1s signals[23]–[25]. From **Fig. 4.4(a),** thermal treatment in N_2 caused a larger Ga contamination, which can be explained using the smaller particulate size estimated by XRD. The smaller size gave the larger surface and/or grain-boundary-like sites to distribute the diffused Ga atoms. This can support the above assumption; however, further consideration is difficult at this stage. Anyway, it can be concluded that the Ga atoms diffused into the ZnO-NPs by the thermal treatment, and, because of the following reasons, a part of them certainly substituted for the Zn atoms, and Ga was activated as donors.

Another reason may due to the difference in the peak position of the Ga3d spectra. In **Fig. 4.4(a)**, the obtained Ga3d peak positions from β-Ga_2O_3(100) single crystal substrate (20.5 eV, i.e., +10.5 eV from Zn3d) and a sputtered Ga-doped ZnO (GZO) film (19.6 eV, i.e., +9.6 eV) are also shown. Generally, the Ga atoms in the GZO film are activated by substituting for the Zn atoms, which will cause the variation of a chemical bonding state and the difference of the peak position in the Ga-related spectra. In the case of "ZnO/Ga_2O_3 mixed (without centrifugal separation)", all the Ga 3d signals originated from the mixed Ga_2O_3 particles, naturally showing a similar peak position with that of

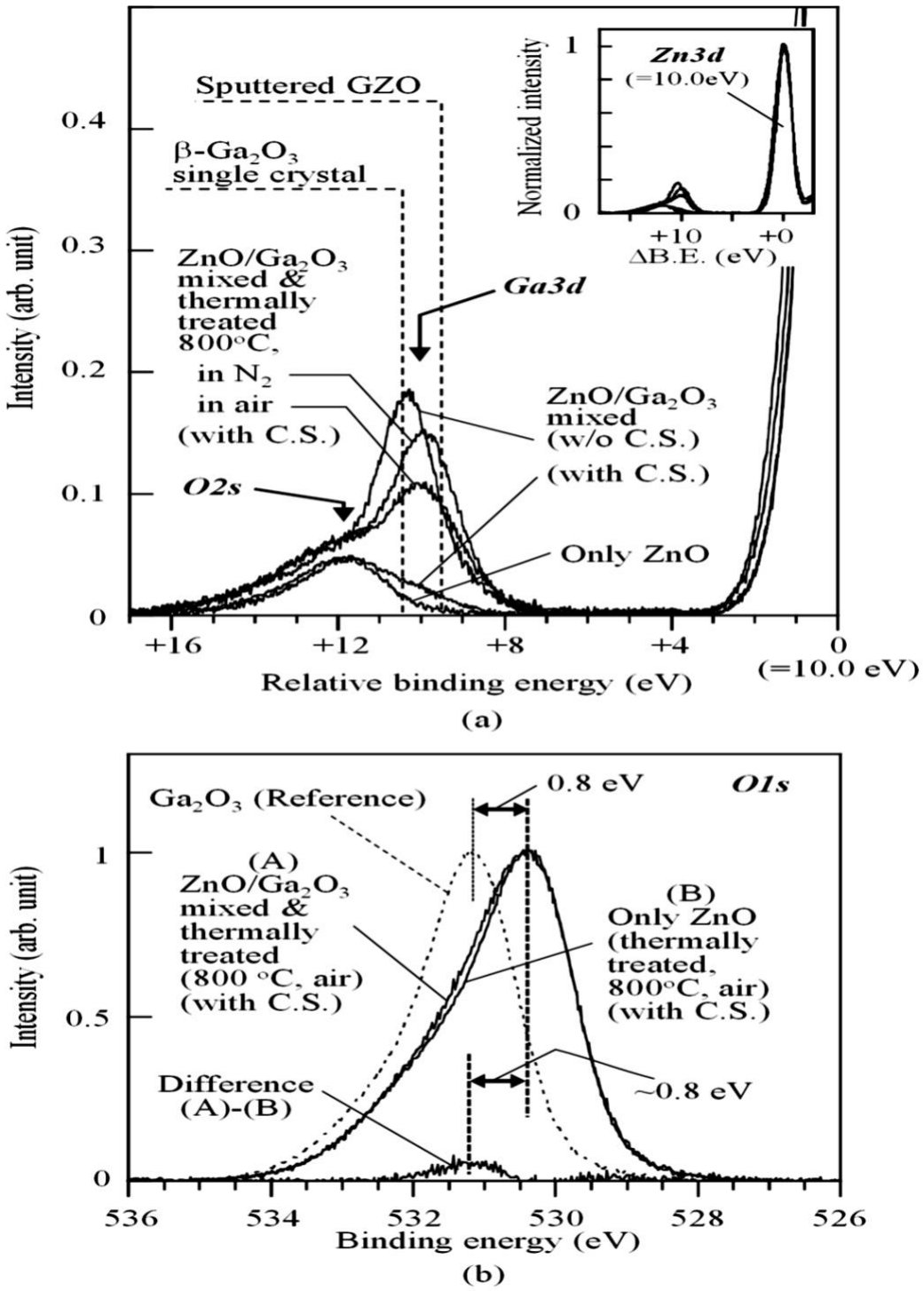

Fig. 4.4 (a) XPS Ga 3d spectra for various samples. The peak position and intensity were normalized with the Zn 3d peak. The inset shows the overall spectra of Zn and Ga 3d. (b) Comparison of XPS O1s spectra between particle layers using thermally treated only-ZnO and ZnO/Ga2O3-mixed particles. As a reference, Ga2O3 O 1s spectrum is also shown. (C.S.: centrifugal separation). Referring [19].

the β-Ga_2O_3 single crystal. On the other hand, in the case of "ZnO/Ga_2O_3 mixed & thermally treated (800°C, with centrifugal separation) in N_2 and the air", the peak position shifted towards the lower binding energies tending to that of the GZO film. However, the peak position is not the same as that of the GZO film, suggesting that some of the diffused Ga atoms substituted for the Zn atoms.

The other reason is a lattice constant variation. The estimated lattice constants using the Bragg's law on the hexagonal system and the accurate peak positions of XRD (002) signals are 5.2057 Å (2θ = 34.415°) and 5.2044 Å (2θ = 34.424°) from **Fig. 4.3(a)** and 4**.3(b),** respectively, i.e., about a 0.001-Å reduction was observed after the thermal treatment with the Ga_2O_3 particles. Generally, the lattice constant will be reduced by the substitution of Ga (0.47 Å) for Zn (0.60 Å) because of a smaller ion radius[26]. In our case, the observed change was small, but this can also explain that some of the diffused Ga atoms substituted for the Zn atoms.

From the XRD and XPS analyses, direct Ga-doping to ZnO-NPs by simple mixing and thermal treating with Ga_2O_3 particles was confirmed, which reduced the resistivity of the sprayed ZnO NP-layers dramatically.

Finally, as described in the optical properties section, it was expected that the thermal treatment in pure N_2 tended to generate more defects compared to the open air, which would act as native donors improving the conductance. However, the obtained sheet resistances tended to show the opposite behavior. One possible reason is that the oxygen vacancies were generated mainly at the surfaces of NPs, which cannot contribute to the generation of carriers different from the bulk. Another possible reason is that the defects were not generated as expected. Recent photoluminescence analyses (not shown here) support the latter case, i.e., the thermal treatment in the pure N_2 ambient leads less defects compared with that in the open air. Controlling the defects is important for the diffusion and substitution behaviors. So, it needs continuous investigation about the defect properties on ZnO-NPs to achieve more effective Ga-doping.

4.4 Chapter Conclusions

The detailed analyses of XPS and XRD results revealed that the expected Ga-doping and the improved crystallite size of ZnO-NPs were confirmed by mixing and thermally treating with Ga_2O_3 particles at 800°C in the air using our diffusion type Ga-doping process, resulting in the dramatic reduction of the sheet resistances of the sprayed n-ZnO NP-layers has been seen. The result of sheet resistance was confirmed as 800°C becoming the optimal temperature during annealing, depending on ambient gas (air and N_2).

4.5 References

[1] G. Luo, H. Li, L. Gao, D. Zhang, and T. Lin, "Porous structured niobium pentoxide/carbon complex for lithium-ion intercalation pseudocapacitors," *Mater. Sci. Eng. B Solid-State Mater. Adv. Technol.*, vol. 214, pp. 74–80, 2016, doi: 10.1016/j.mseb.2016.09.004.

[2] Y. H. Kim, E. Y. Lee, H. H. Lee, and T. S. Seo, "Characteristics of Reduced Graphene Oxide Quantum Dots for a Flexible Memory Thin Film Transistor," *ACS Appl. Mater. Interfaces*, vol. 9, no. 19, pp. 16375–16380, 2017, doi: 10.1021/acsami.7b00714.

[3] R. N. Bukke, J. K. Saha, N. N. Mude, Y. Kim, S. Lee, and J. Jang, "Lanthanum Doping in Zinc Oxide for Highly Reliable Thin-Film Transistors on Flexible Substrates by Spray Pyrolysis," *ACS Appl. Mater. Interfaces*, vol. 12, no. 31, pp. 35164–35174, 2020, doi: 10.1021/acsami.0c05151.

[4] Z. Meric, C. Mehringer, M. P. M. Jank, W. Peukert, and L. Frey, "Electrical properties of solution processed layers based on Ge-Si alloy nanoparticles," *MRS Adv.*, vol. 1, no. 33, pp. 2331–2336, 2016, doi: 10.1557/adv.2016.329.

[5] S. C. Lim *et al.*, "Electrical properties of solution-deposited ZnO thin-film transistors by low-temperature annealing," *J. Nanosci. Nanotechnol.*, vol. 14, no. 11, pp. 8665–8670, 2014, doi: 10.1166/jnn.2014.10002.

[6] T. Yoshida, K. Shinohara, D. Itohara, and Y. Fujita, "Effects of thermal pressing on ZnO nanoparticle layers deposited by drop casting," *e-Journal Surf. Sci. Nanotechnol.*, vol. 14,

no. May, pp. 175–178, 2016, doi: 10.1380/ejssnt.2016.175.

[7] M. S. Rajachidambaram *et al.*, “Formation of zinc oxide films using submicron zinc particle dispersions,” *J. Vac. Sci. Technol. B, Nanotechnol. Microelectron. Mater. Process. Meas. Phenom.*, vol. 30, no. 4, p. 041805, 2012, doi: 10.1116/1.4731255.

[8] N. Mechau, S. Bubel, D. Nikolova, and H. Hahn, “Influence of stabilizers in ZnO nano-dispersions on the performance of solution-processed FETs,” *Phys. Status Solidi Appl. Mater. Sci.*, vol. 207, no. 7, pp. 1684–1688, 2010, doi: 10.1002/pssa.200983768.

[9] Z. Gao and P. Banerjee, “Review Article: Atomic layer deposition of doped ZnO films,” *J. Vac. Sci. Technol. A*, vol. 37, no. 5, p. 050802, 2019, doi: 10.1116/1.5112777.

[10] H. Faber *et al.*, “Morphological impact of zinc oxide layers on the device performance in thin-film transistors,” *Nanoscale*, vol. 3, no. 3, pp. 897–899, 2011, doi: 10.1039/c0nr00800a.

[11] H. C. Huang and T. E. Hsieh, “Highly stable precursor solution containing ZnO nanoparticles for the preparation of ZnO thin film transistors,” *Nanotechnology*, vol. 21, no. 29, 2010, doi: 10.1088/0957-4484/21/29/295707.

[12] S. Lee, Y. Jeong, S. Jeong, J. Lee, M. Jeon, and J. Moon, “Solution-processed ZnO nanoparticle-based semiconductor oxide thin-film transistors,” *Superlattices Microstruct.*, vol. 44, no. 6, pp. 761–769, 2008, doi: 10.1016/j.spmi.2008.09.002.

[13] F. F. Vidor, T. Meyers, and U. Hilleringmann, “Inverter circuits using ZnO nanoparticle based thin-film transistors for flexible electronic applications,” *Nanomaterials*, vol. 6, no. 9, pp. 1–15, 2016, doi: 10.3390/nano6090154.

[14] Y. Fujita, K. Moriyama, Y. Hiragino, Y. Furubayashi, H. Hashimoto, and T. Yoshida, “Electroluminescence from nitrogen doped ZnO nanoparticles,” *Phys. Status Solidi Curr. Top. Solid State Phys.*, vol. 11, no. 7–8, pp. 1260–1262, 2014, doi: 10.1002/pssc.201300645.

[15] K. Senthilkumar, T. Yoshida, and Y. Fujita, “Formation of D–VZn complex defects and possible p-type conductivity of ZnO nanoparticle via hydrogen adsorption,” *J. Mater. Sci.*, vol. 53, no. 17, pp. 11977–11985, 2018, doi: 10.1007/s10853-018-2498-7.

[16] D. Itohara, K. Shinohara, T. Yoshida, and Y. Fujita, “P-Channel and n-Channel Thin-Film-Transistor Operation on Sprayed ZnO Nanoparticle Layers,” *J. Nanomater.*, vol. 2016, no. Dc, 2016, doi: 10.1155/2016/8219326.

[17] V. I. Nefedov, Y. V. Salyn, G. Leonhardt, and R. Scheibe, “A comparison of different spectrometers and charge corrections used in X-ray photoelectron spectroscopy,” *J. Electron Spectros. Relat. Phenomena*, vol. 10, no. 2, pp. 121–124, 1977, doi: 10.1016/0368-2048(77)85010-X.

[18] O. Lupan *et al.*, “Synthesis and characterization of ZnO nanowires for nanosensor applications,” *Mater. Res. Bull.*, vol. 45, no. 8, pp. 1026–1032, 2010, doi: 10.1016/j.materresbull.2010.03.027.

[19] T. Yoshida, I. M. Maruful, and Y. Fujita, “Trial of Ga-doping on ZnO nanoparticles by thermal treatment with Ga2O3 nanoparticles,” *e-Journal Surf. Sci. Nanotechnol.*, vol. 18, pp. 12–17, 2020, doi: 10.1380/EJSSNT.2020.12

[20] S. M. Liu, F. Q. Liu, H. Q. Guo, Z. H. Zhang, and Z. G. Wang, “Correlated structural and optical investigation of terbium-doped zinc oxide nanocrystals,” *Phys. Lett. Sect. A Gen. At. Solid State Phys.*, vol. 271, no. 1–2, pp. 128–133, 2000, doi: 10.1016/S0375-9601(00)00341-8.

[21] A. A. Azab, E. E. Ateia, and S. A. Esmail, “Comparative study on the physical properties of transition metal-doped (Co, Ni, Fe, and Mn) ZnO nanoparticles,” *Appl. Phys. A Mater. Sci. Process.*, vol. 124, no. 7, pp. 1–10, 2018, doi: 10.1007/s00339-018-1871-3.

[22] J. J. Shan, C. H. Li, J. M. Wu, J. A. Liu, and Y. S. Shi, “Shape-controlled synthesis of monodispersed beta-gallium oxide crystals by a simple precipitation technique,” *Ceram. Int.*, vol. 43, no. 8, pp. 6430–6436, 2017, doi: 10.1016/j.ceramint.2017.02.056.

[23] N. Tabet, M. Faiz, and A. Al-Oteibi, “XPS study of nitrogen-implanted ZnO thin films obtained by DC-Magnetron reactive plasma,” *J. Electron Spectros. Relat. Phenomena*, vol. 163, no. 1–3, pp. 15–18, 2008, doi: 10.1016/j.elspec.2007.11.003.

[24] T. V. Richter *et al.*, “Room temperature vacuum-induced ligand removal and patterning of ZnO nanoparticles: From semiconducting films towards printed electronics,” *J. Mater. Chem.*, vol. 20, no. 5, pp. 874–879, 2010, doi: 10.1039/b916778c.

[25] L. G. Mar, P. Y. Timbrell, and R. N. Lamb, “An XPS study of zinc oxide thin film growth on copper using zinc acetate as a precursor,” *Thin Solid Films*, vol. 223, no. 2, pp. 341–347, 1993, doi: 10.1016/0040-6090(93)90542-W.

[26] H. Gómez and M. de la, “Ga-doped ZnO thin films: Effect of deposition temperature, dopant concentration, and vacuum-thermal treatment on the electrical, optical, structural and morphological properties,” *Mater. Sci. Eng. B Solid-State Mater. Adv. Technol.*, vol.

134, no. 1, pp. 20–26, 2006, doi: 10.1016/j.mseb.2006.07.039.

5. Optimization of Ambient Atmosphere for Ga-Doping and its Application to TFT Channel Layers

5.1 Introduction

Using semiconductor nanoparticles (NPs) the formation of channel layers of thin-film transistors (TFTs) with coating techniques is an attractive technology because of the high selectivity of substrate materials, surface morphology, low cost, and large process area[1]–[4]. ZnO is the subject of numerous ongoing studies because of exceptional properties such as increased chemical and thermal stability—even when surrounded by hydrogen plasma—as compared with other oxides (e.g., SnO_2 and ITO), wide band gap[5], large exciton binding energy of 60 meV at room temperature[6], non-toxicity, and low costs. These attributes, combined with its applications in a wide variety of fields such as electronics, optics, optoelectronics, and conversion photovoltaics [7], [8], make it a model material.

The presence and operation of both n/p-channel back-gate TFTs on Si/SiO_2 substrates have recently been demonstrated[9] employing laboratory-synthesized ZnO NPs[10]. However, the channel resistivity of NP layers was too high, inhibiting the TFT's performance. Impurity doping such as Group III elements can be effective to reduce the resistivity of n-type ZnO NPs[11]. In a detailed review of doped ZnO, Gao et al. concluded that Ga-doped ZnO obtained a low resistive NP layer as well as improved electrical properties among various doping elements[12]. Indeed, for ZnO films, various Ga-doping attempts have been made with many successes[13], e.g., magnetron sputtering[14], chemical vapor deposition (CVD)/atomic layer deposition (ALD)[15]–[17], chemical solution deposition (CSD) including the sol-gel method[18], and Various techniques have been used in the preparation of ZnO thin films[19]. These deposition methods are highly applicable for the fabrication of thin films; however, these methods are inapplicable for particle processing such as solution-based deposition process. Several discoveries on thermal-diffusion-type Ga-doping utilizing a multilayer system imply that Ga-doping into ZnO NPs could be achieved through a diffusion mechanism[20]. In light of the foregoing, our group has previously tried Ga doping into ZnO NPs utilizing the thermal diffusion methodology with Ga_2O_3 NPs and fabricate spray coated NP layers onto

glass substrates[21]. Our unique Ga-doping process showed a dramatic reduction of sheet resistance with a temperature of 800°C or greater; however, specific variables like the ambient effect in the thermal process and the doping mechanisms were not optimized.

In this study, Ga was doped into ZnO NPs in a way that approximated thermal diffusion utilizing Ga_2O_3 NPs under various atmospheric conditions. Spray-coated ZnO:Ga NP-layers with low resistivity were obtained, and the structural, optical, and electrical properties of the material were examined. Furthermore, for further investigation of Ga-doping, depletion-type Schottky-gate TFTs were fabricated using the obtained ZnO:Ga NP-layers.

3) **The major part of this chapter has been published to ‘‘Coatings’’ MDPI (**I.M.Maruful, Toshiyuki Yoshida, and Yasuhisa Fujita. 2022. "Effects of Ambience on Thermal-Diffusion Type Ga-Doping Process for ZnO Nanoparticles" *Coatings* 12, no. 1: 57. https://doi.org/10.3390/coatings12010057)**.**

5.2 Experimental details

An arc-discharge-mediated gas evaporation technique was used to synthesize ZnO NPs. A commercially available zinc (4N) rod (metal Zn 99.99 %) was employed as the zinc source, dry air was used as the oxygen source, and a carbon rod functioned as the cathode in the arc plasma process[10]. The pressure inside the chamber was regulated at around 610 Torr using a rotary vacuum pump and a 20 A arc current was produced. A flow controller was used to provide a 5 L/min flow of dry air through the chamber (suppressing nitrogen doping mode). This fabricating condition has the lowest N_2 concentration (approximately 0.01 wt%), while condition 60A has the highest concentration (about 0.31 wt%)[22]. The aforementioned conditions (610 Torr, 20A) were used to generate n-type ZnO NPs (commonly termed as as-prepared ZnO), which were the principal type of ZnO NPs employed in this study.

Ga-doping was carried out by adding 0.06 g of Ga_2O_3 NPs (Sigma-Aldrich Co. Ltd.) with 0.2 g of ZnO NPs and annealed at 800°C for 60 min in atmospheric air (high humid condition) including atmospheric N_2 and O_2; wet air; pure N_2; pure O_2; and dry air

(designated “ZnO:Ga-open air”, “ZnO:Ga-wet air”, “ZnO:Ga-N_2”, “ZnO:Ga-O_2”, and “ZnO:Ga-dry air”, respectively). Wet air is defined as air that has a relative humidity of about 100 percent and is produced by water bubbling. The dispersions were uniformly dispersed 0.26 g of the aforementioned annealed NPs in 10 g of water with an ultrasonic homogenizer (150 W, 3 min, 20 kHz) and centrifuging them (3000 G, 1 min) to remove residual Ga_2O_3 NPs. As a result, practically all of the residual Ga_2O_3 particles were successfully removed, and big ZnO NPs were precipitated. Seven milliliters of the dispersion were sprayed on a quartz substrate at 5 s intervals for ~15 min, where the hot plate temperature keeps constant at 500°C. An airbrush spray coating technique was employed to sinter the NPs and avoid aggregation. The top-gate metal-semiconductor (MES) field-effect-transistor (FET) ZnO NP TFTs were employed in this study. The n-type ZnO NP channel layer (~1 μm) was grown on a glass substrate by spray coating, and Al evaporation (~50 nm) was used as the source (S) and drain (D) ohmic contacts. Finally, a gold Schottky gate electrode (~30 nm) was fabricated between the S and D contacts using a sputter.

Al/Au electrodes with a width and distance of 0.3 mm were deposited onto the sprayed NPs layer for the two-probe (*I*–*V*) measurements. To determine the contact resistance, sheet resistances, and TFT output characteristic, *I*–*V* measurements were carried out using a shielding probe system. An E5270B precision measurement mainframe with an E5287A Atto-level high-resolution SMU module (Keysight Technologies) was used to determine such properties. A field-emission scanning electron microscope (FESEM; JSM-7001FA, JEOL, 5 kV) & Powder X-ray diffraction (SmartLab, Rigaku Corporation, $\lambda = 0.154$ nm) was used to measure the Surface and structural properties of sprayed NPs layer. To measure the optical properties of sprayed NP layers, a Fluromax-4 spectrofluorometer (Horiba Advanced Techno Co. Ltd.) was used. The photoluminescence (PL) spectra were taken with a 325 nm excitation wavelength and a 0.2 s exposure time, and the defect spectra were analyzed using origin lab pro software.

5.3 Experimental results and discussion

5.3.1 Nano-particle size distribution

The particle size distributions of laboratory synthesized ZnO NPs and Ga_2O_3 NPs after being mixed and thermally treated at 800°C under various atmospheres are shown in **Fig. 5.1**, which were prepared by dispersing each particle in ultrapure water by ultrasonic homogenizer without centrifugal separation procedure. The result revealed that the particles have sharp distribution with a median size of 97.2, 130.9, 100.7, and 115.6 nm for as-prepared ZnO, ZnO:Ga-air, ZnO:Ga-N_2, and ZnO-Ga-O_2 respectively. The variation of particle distribution clearly indicates the effect of thermal treatment in the NPs under various atmospheres during annealing.

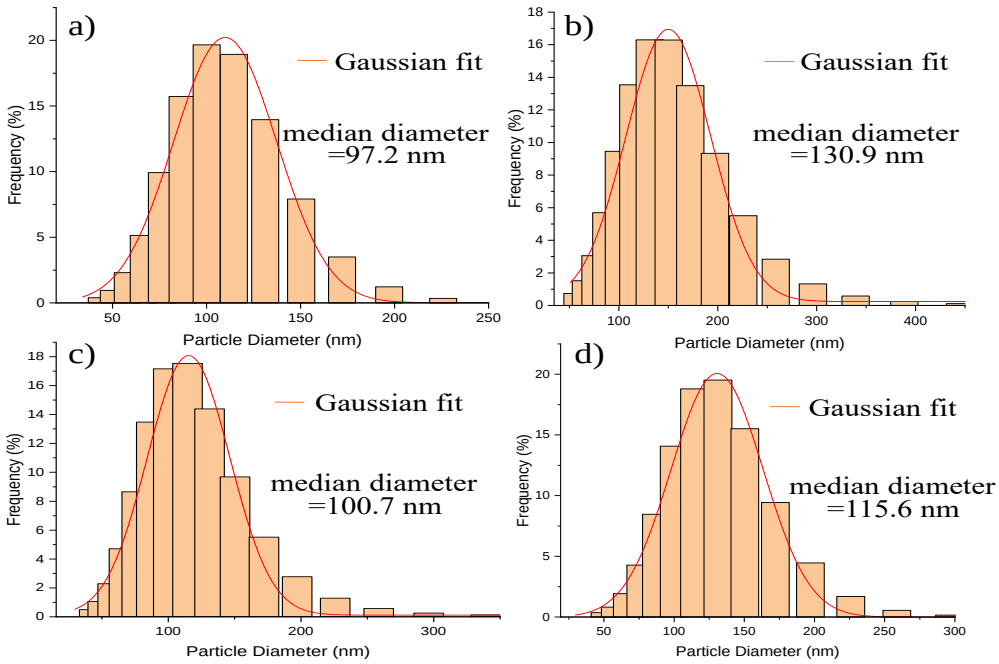

Figure 5.1 Nano-particle distribution curve of (a) as-prepared ZnO (b) ZnO:Ga-air, (c) ZnO:Ga-N_2, (d) ZnO-Ga-O_2.

5.3.2 Surface Morphology

The surface morphologies of the as-prepared ZnO, ZnO:Ga-open air, ZnO:Ga-N_2, and ZnO:Ga-O_2 layers were studied using scanning electron microscopy (SEM) shown in fig **5.1**. These images depict the surfaces as having developed uniformity after the Spray process. By maintaining a high surface temperature at the time of spraying, the solvent (H_2O in this study) evaporated immediately, which reduced the movement of the ZnO NPs and thus suppressed their aggregation. The roughness of NP layer was measured using scanning probe microscopy/dynamic force mode (SPM/DFM) surface characterization technique and the image depicts that the sample of as-prepared ZnO had a surface roughness of 267.6 nm shown in **Fig. 5.2**. The scanning was done in a 30 x 30 µm area, and the roughness is mostly found at the corner, which could be attributable to noise. However, because the roughness of the thin-film technology is rather significant, the flow of current between source and drain can impede due to this rough surface. The variations in particle distribution were within 34 nm in the DLS measurement, and the surface roughness of the other Ga-doped ZnO NPs surfaces was comparable to that of as-prepared ZnO when compared to the original surface roughness.

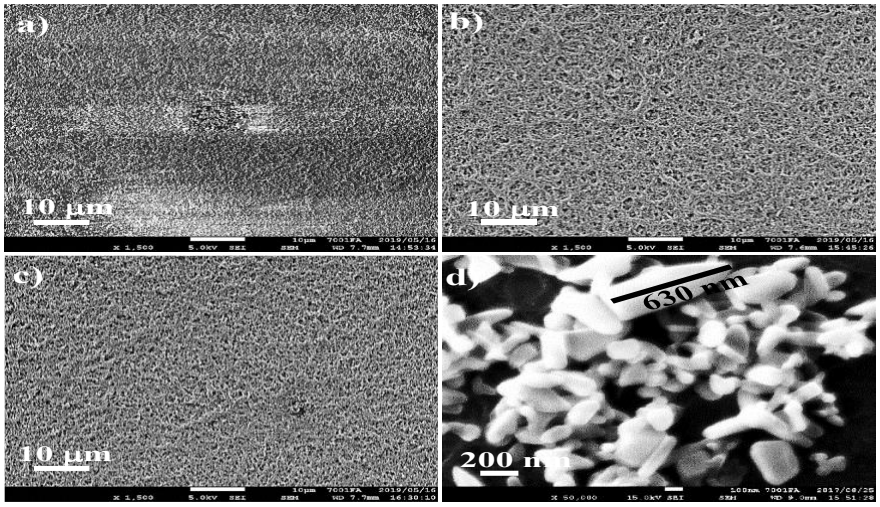

Figure 5.1 SEM image of the (a) ZnO:Ga-air, (b) ZnO:Ga-N_2, (c) ZnO-Ga-O_2 and, (d) as-prepared ZnO.

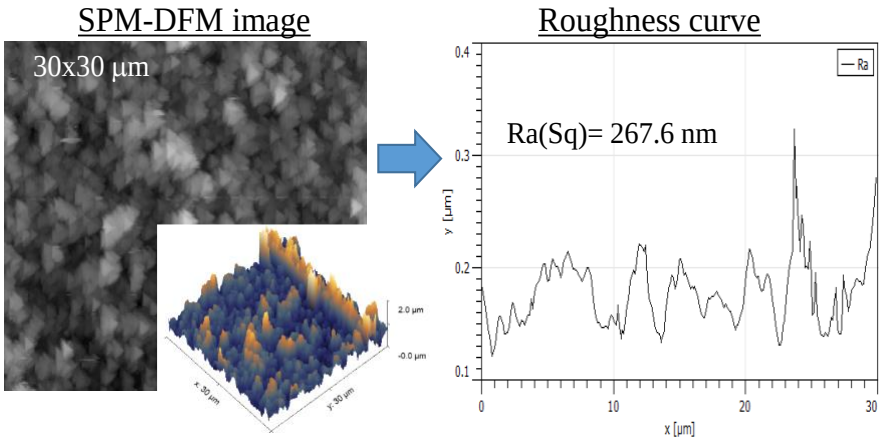

Figure 5.2 SPM-DFM image and the roughness curve of as-prepared ZnO

5.3.3 Electrical properties

A two-probe approach was used to measure the electrical characteristics of the ZnO layers. The sample is shielded from light by being placed in the shield box, and the two probes are brought into contact with the Al/Au electrodes to measure the sample's conductivity throughout a -10 V to 10 V range. The sheet resistance (R_S) was calculated using Eq. (1) from the slope of the *I–V* curves using 0.3 mm x 0.3 mm square electrodes placed 0.3 mm apart.

$$R_s = \frac{R_M * W}{L} \qquad (1)$$

where R_M is the measured resistivity, W is the width, and L is the distance. **Fig 5.2** shows the calculated sheet resistance values for several sprayed-NP layers across several distributions. Here, "ZnO-open air" refers to a sprayed NP-layer made of ZnO-NPs that have been annealed in the open air without the use of Ga_2O_3 NPs, emphasizing the necessity of thermal treatment without Ga doping. The average sheet resistances of the as-prepared ZnO, ZnO-open air, ZnO:Ga-open air, ZnO:Ga-wet air, ZnO:Ga-N_2, ZnO:Ga-O_2, and ZnO:Ga-dry air layers were found to be 4.6×10^6, 6.8×10^9, 8.0×10^2, 8.8×10^2, 7.5×10^5, 7.5×10^7, and 3.9×10^9 Ω/sq, respectively. While previous research

has shown that resistivity is dependent on annealing temperature [23], this research tried to show that resistivity caused by Ga-doping is dependent on the

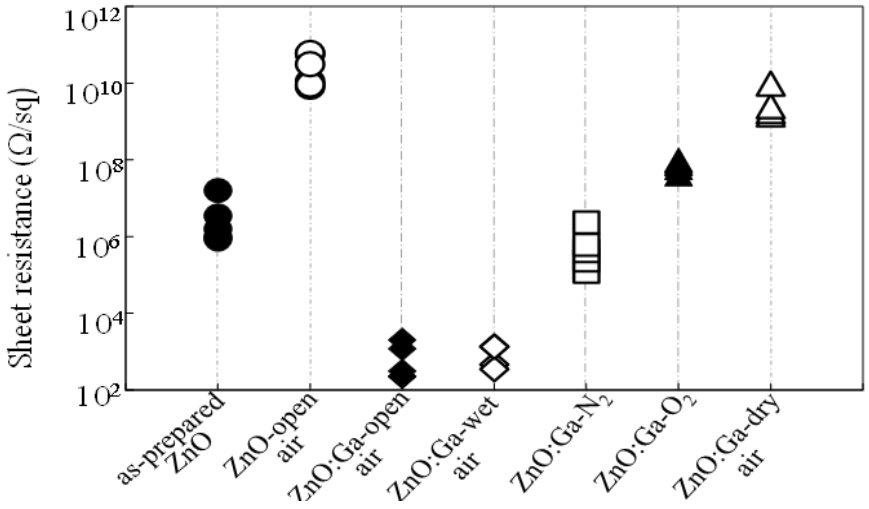

Figure 5.2. Resistivity distribution graph for each sprayed NPs layer. Referring [23].

annealing atmosphere. The resistivity distribution graph demonstrates that the ZnO:Ga-open air and ZnO:Ga-wet air layers have the lowest resistivity. After thermal annealing, without Ga diffusion, the resistivity of the ZnO-open air NPs layer was remained high, which may due to the reduction of electron carriers with re-oxidation of oxygen vacancy[23]. All Ga-diffused samples show a decrease in resistivity when compared to the resistivity of the ZnO-open air layer, confirming that the characteristics of the ZnO particles were impacted by Ga thermal diffusion. Especially, the resistance decrease for ZnO:Ga-open air and ZnO:Ga-wet air layers was particularly considerable, reaching the order of sub-k Ω/sq, whereas the resistivity of the other three types of layers remained high. When compared to the ZnO-open air layer, the ZnO:Ga-N_2 layer had a lower resistance value; however, only this layer did not contain oxygen gas during the thermal process, preventing re-oxidation of oxygen vacancies. As a result, the sheet resistance value of the ZnO:Ga-N_2 layer can be comparable with the ZnO as-prepared samples. The ZnO:Ga-open air and ZnO:Ga-wet air layers only showed a significant reduction of sheet

resistance. The presence of humidity during the Ga-doping using thermal diffusion process is the only plausible distinction here.

The electrical properties of the sprayed NP layers as characterized by the Hall effect are summarized in **Table 5.1**. All of the samples had n-type conductivity. In ZnO:Ga-open air samples, the electron concentrations improved dramatically, indicating that the Ga atoms effectively diffused into the Zn site. In ZnO, the enhanced carrier concentration is due to the free electrons/holes donated by doping ions. As a result, incorporating donors in the ZnO layers enhanced the carrier concentration. The minimum resistance and the highest carrier concentration occur simultaneously in Ga doped ZnO with n-type conductivity, especially in air annealed samples. The Hall mobility of sprayed NP layers is increased and decreased based on the sheet resistance. For the lowest sheet resistance, the Hall mobility was found to be increased. The increase in mobility is attributed to a decrease in the scattering mobility of ionized impurities. The measured resistivity of the NP layers is considerably high as compared to the two-probe measurement, but a similar trend has been observed. The lowest career concentration, as well as the maximum sheet resistance, were observed for the undoped ZnO NPs layer, clearly confirming the Ga-doping effects.

Table 5.1: Hall measurement

Sample	Career Concentration (cm^3)	Mobility (cm^2/V-s)	Resistivity (Ω/sq)
As-prepared ZnO	1.30×10^{10}	2.9	1.70×10^{11}
ZnO:Ga-open air	6.89×10^{16}	46.2	2.49×10^{7}
ZnO:Ga-N_2	2.00×10^{12}	13.2	1.10×10^{10}
ZnO:Ga-O_2	7.10×10^{11}	0.47	4.00×10^{10}

5.3.4 Structural properties

X-ray diffraction (XRD) was used to determine the structural properties of the sprayed NP layers, and the results revealed that all NPs had a hexagonal wurtzite crystal structure[24], [25], which corresponded to the space group P63mc (No. 186, JCPDS No. 79–0208) shown in **Fig 5.3. (a)**. All samples had strong peak intensity along (100) and (101), and a relatively weaker peak was observed along (002) *hkl* plane. The crystalline dimensions of 2θ along the *a*-axis and the *c*-axis were approximately 31.78˚ and 34.42°, respectively, for all samples. The strong (100) peak suggested that the deposited layers

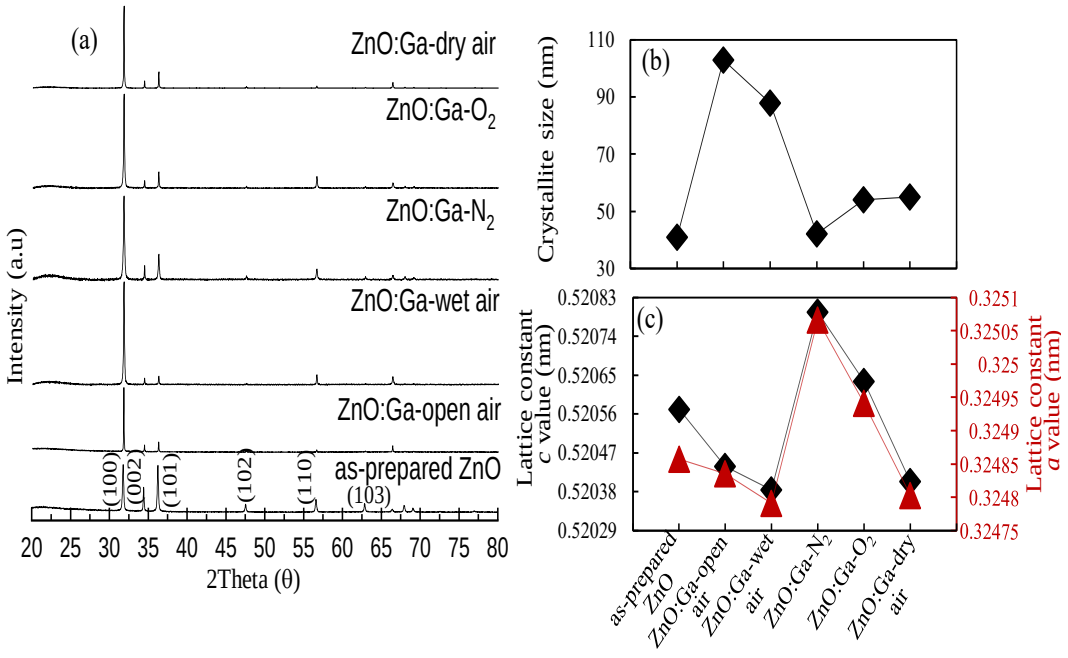

Figure 5.3 (a) X-ray diffraction patterns of spray coated NP layers, (b) the calculated crystallite size, and (c) lattice constant for *a* and *c* value. Referring [23].

had a preferred orientation with the *a*-axis perpendicular to the substrate[26] and the crystal structure of sprayed NPs layer was reliant on its thermal environment. The diffraction angle of (002) peak position was observed at 34.414° for all cases which is slightly lower than the corresponding value 34.467° for bulk ZnO (COD 10 11 258)[27]. This was attributed to a reduction of surface effects, resulting in lattice deformations and an increase in the lattice constant along the c-axis[28]. The intensity of the thermally Ga-

diffused NP samples was comparatively higher, indicating enhanced crystallite growth and crystallinity. This was partly due to Ga^{3+} being integrated into the ZnO matrix as substitutional impurities on the Zn lattice sites at this annealing temperature[29]. The coalescence of those crystallites that were contiguous with air molecules is responsible for the low full-width-at-half-maximum (FWHM) value for ZnO:Ga-open air. Using Scherrer's formula, as given in Eq. (2)[30], the crystallite size (D) of the sprayed layers was calculated from the FWHM values based on the (100) peaks, with the findings shown in Figure **5.3. (b).**

$$D = \frac{0.9\lambda}{\beta cos\theta}, \qquad (2)$$

where λ is the wavelength of the incident XRD, β is the FWHM in radians, and θ is the Bragg angle of the diffraction peak. The crystallite sizes of the as-prepared ZnO, ZnO:Ga-open air, ZnO:Ga-wet air, ZnO:Ga-N_2, ZnO:Ga-O_2, and ZnO:Ga-dry air layers were found to be 41, 103, 88, 42, 54, and 55 nm, respectively. The crystallite sizes increased for Ga-doped NPs layer during annealing, particularly when annealing was performed in the open air and the wet air atmospheric conditions. After Ga-doping and annealing, the significant development of crystallite structure occurs in nanoparticles due to the atoms move to an inclinable position and tend to interact with nearby crystallites, resulting in the formation of large crystallites. The crystallite size of the thermal-diffused Ga-doped NP layers was larger than that of as-prepared ZnO, this was because of the smaller lattice deformation after annealing. This outcome is primarily due to the fact that the atomic radii of Ga and Zn are similar[25]. The density of boundaries between crystallites increased due to the smaller crystallite size of the sprayed NPs layer, resulting in a higher resistivity of the conducting layer. The crystallite size increased during annealing, resulting in reduced crystallite boundaries and lower resistivity. Bragg's law ($2dsin\theta = n\lambda$) and the relationship formula (Eq. 3)[31] were used to obtain lattice constants *a* and *c*:

$$\frac{1}{d^2_{hkl}} = [\frac{4}{3}(h^2+k^2+hk)+l^2(\frac{a}{c})^2]\frac{1}{a^2}, \qquad (3)$$

where d_{hkl} is the interplanar spacing calculated from Bragg's equation, and *h*, *k*, and *l* are the Miller indices. The lattice parameters usually rely on several factors such as free-electron concentration, the concentration of doping atoms, defects, the variation of ionic

radii concerning the substituted matrix ion, external strains by substrate, and temperature. The lattice parameters for the as-prepared ZnO layer were found to be a = 3.2485 Å and c = 5.2057 Å, while the lattice constant of ZnO was reported in the range from 3.2475 Å to 3.2501 Å for the "a" parameter and from 5.2042 to 5.2075 for the "c" parameter[32]. Based on the doping elements, doping concentration, thermal temperature, thermal atmospheres, these values can be varied. The calculated lattice constant values in Armstrong (Å) are shown in **Fig. 5.3 (c)** and the results depict that the lattice constant values of "a" and "c" were found to be decreased phenomenon in ZnO:Ga-open air and ZnO:Ga-wet air layers compared to as-prepared ZnO.

This result indicates the incorporation of Ga atoms substituting Zn atoms effectively because of smaller ionic radii of Ga (0.47 Å) than that of Zn (0.60 Å)[31]. Based on these findings, the results also demonstrate that Ga was also successfully diffused in the ZnO:Ga-O_2 layer; however, other factors such as the high density of crystallite boundaries as determined by the XRD spectrum and the low crystallinity as determined by the suppressed PL intensity explained below have deteriorated the ZnO:Ga-O_2 layer's current transporting possibility. Further research is necessary to determine how these mechanisms affected the ZnO:Ga-O_2 layer's lattice constant.

5.3.5 Optical properties

To identify the material defects and impurities by analyzing the luminescence spectrum the PL study was investigated and the spectra of the as-prepared ZnO, ZnO:Ga-open air, ZnO:Ga-N_2, ZnO:Ga-O_2, ZnO:Ga-wet air, and ZnO:Ga-dry air layers are shown in **Figure 5.4 (a).** The spectra consisted of ultraviolet (UV) region at a wavelength of 376–384 nm called edge luminescence and a broad emission band in the visible range at 450–550 nm called green luminescence. The variation of the UV peak intensity is also shown in the inset of **Fig 5(a)**. In PL spectra, the enhanced UV emissions induced by crystalline improvement of the NPs layer and the red-shift phenomena of UV peak intensity may induced by exciton and donor-acceptor (D–A) pair emissions: Layers of Ga-open air and ZnO:Ga-wet air. These results predominantly indicate successful Ga-doping particularly in these two samples, where a considerable reduction in sheet resistance values was also

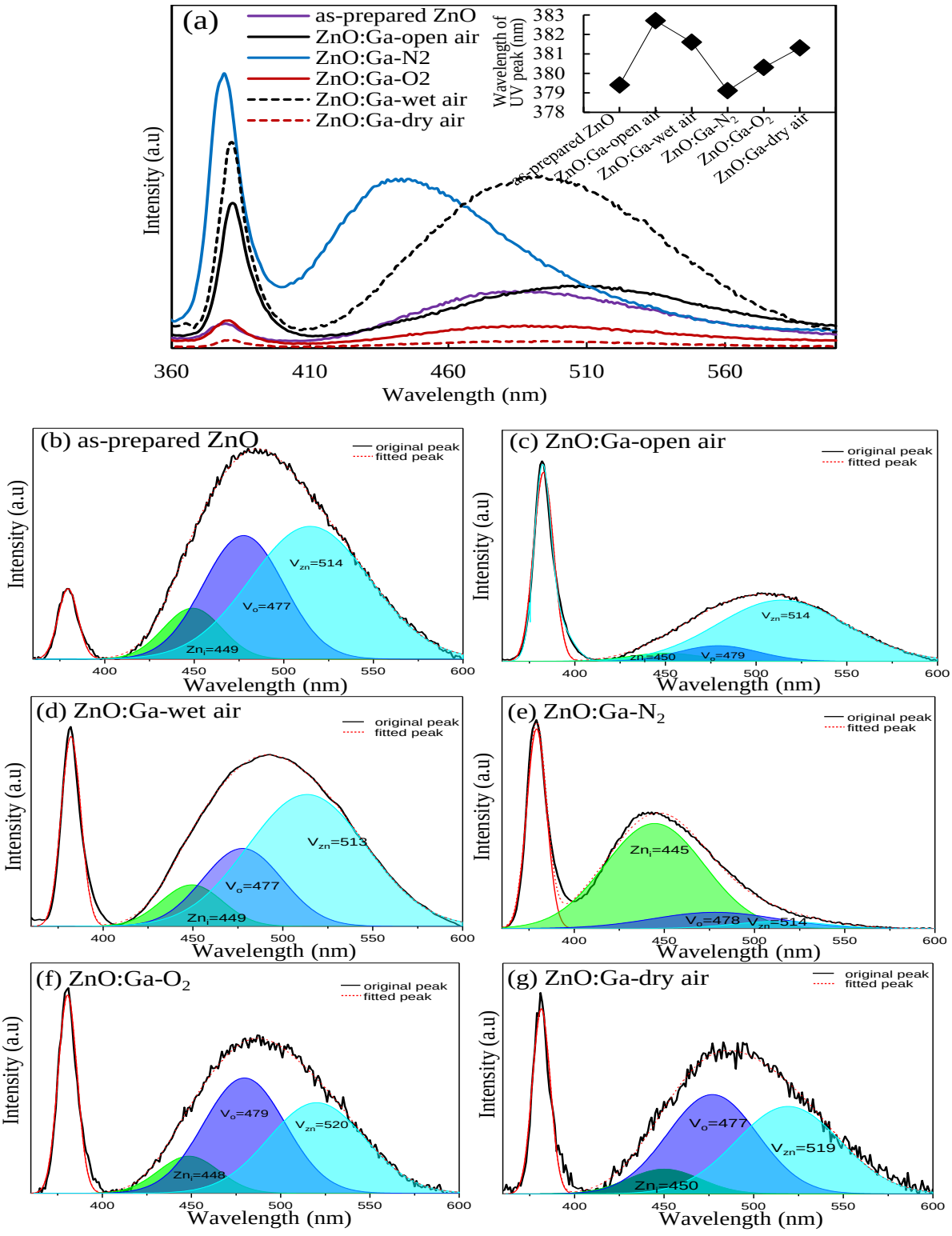

Figure 5.4 (a) Photoluminescence (PL) spectra, and deconvoluted PL spectra of (b) as-prepared ZnO, (c) ZnO:Ga-open air, (d) ZnO:Ga-wet air, (e) ZnO:Ga-N_2, (f) ZnO:Ga-O_2, and (g) ZnO:Ga-dry air. Referring [23].

seen in two-probe measurements as shown in **Fig. 5.2**. The UV peak intensity of ZnO:Ga-dry air layer exhibited red-shifting similar to that of the ZnO:Ga-wet air layer, however, the luminescence intensity was too low which may could be owing to high density non-radiative recombination levels, such as NP surface defects, which could explain why the conductivity did not improve. The surface state density of the NPs will be compared in the future. To investigate the defect mechanism in more detail, the green luminescence from the PL spectra was deconvoluted using the Gaussian function distribution, as shown in **Fig. 5.4 (b) ~ 5.4 (g)**. The native defects of various ZnO samples in PL spectra may differ from sample to sample, as it is mostly determined by the sample's particular history, such as synthesis process, thermal treatment, and so on. In addition, the positions of defect emissions can alter and even combine under different conditions (e.g., n-/p-type doping, annealing temperature/atmosphere/pressure, and Zn/O-rich). Based on the above considerations, we deconvoluted the PL spectra that consist of four sub-bands located at 382(±3) nm, 449(±5) nm, 477(±3) nm, and 514(±6) nm for UV, Zn_i, V_O, and V_{Zn} respectively[33]. Here, the ratio of V_{Zn} in defect components was determined by the FWHM and found to be 81%, 65%, 5%, 43%, and 46% for ZnO:Ga-open air, ZnO:Ga-wet air, ZnO:Ga-N_2, ZnO:Ga-O_2, and ZnO:Ga-dry air, respectively. According to these findings, the V_{Zn} ratios in ZnO:Ga-open air and ZnO:Ga-wet air were substantially higher than those in the other three situations. When ZnO material was annealed at high temperatures (700–900°C) in H_2O ambient, the sublimation of Zn atoms occurs[15], [34]. The sublimation of Zn atoms and the efficient substitution of Ga atoms into the Zn sites might have occurred in parallel in the ZnO:Ga-open air and ZnO:Ga-wet air conditions, indicating that humidity was present in the Ga diffusion process[21]. For ZnO:Ga-N_2, ZnO:Ga-O_2 and ZnO:Ga-dry air, the Ga atoms could not be incorporated into a suitable site, and the crystalline of ZnO NPs was degraded, despite significant Ga diffusion. The XRD spectra in **Figure 4(a)** also stated that, the FWHM ratios of (002) and (101) to (100) hkl plane for the ZnO:Ga-dry air, ZnO:Ga-O_2, and ZnO:Ga-N_2 layers in the 2θ region are different from those of the ZnO:Ga-wet air and ZnO:Ga-open air layers. One possible explanation is that Ga atoms diffused but did not properly substitute Zn sites, preventing crystallite coalescence. Details are still unclear, and further study is needed to adequately model out the entire phenomenon.

To estimate the bandgap of Ga doped ZnO NPs, UV-Vis absorption spectroscopy was carried out. The measurement was performed after dispersing the NPs in ultrapure water. The spectrum reveals a characteristic absorption peak of as-prepared ZnO and ZnO:Ga-open air at the wavelength 371 and 373 nm, respectively. which can be assigned to the intrinsic free exciton absorption of ZnO due to the electron transition from the valance band to the conduction band ($O_{2p} \rightarrow Zn_{3d}$)[35].

Bang gap (E_g) is the summation of exciton energy (E_{ex}) and binding energy (E_b), in the case of direct bandgap ZnO; $E_g = E_{ex}+E_b$ (60meV).

The roughly estimated bandgap for as-prepared ZnO is 3.40eV which is slightly higher than Ga doped ZnO (3.38eV), assuming that the impurity doping is not so much affect the exciton binding energy. However, this difference is comparable to the error in our system, and it is just doping, not making alloy, and the doping amount is less. Burstein–Moss effect is not observed in the transmission spectrum cause the conduction band is fully occupied by the electron, which is obvious from the PL, Abs., and XRD results (High intensity, exciton emission, and the large crystallite size). So, it is suitable to conclude that the variation of the bandgap was less by the Ga-doping process. The absorbance spectra are shown in **Fig. 5.5.**

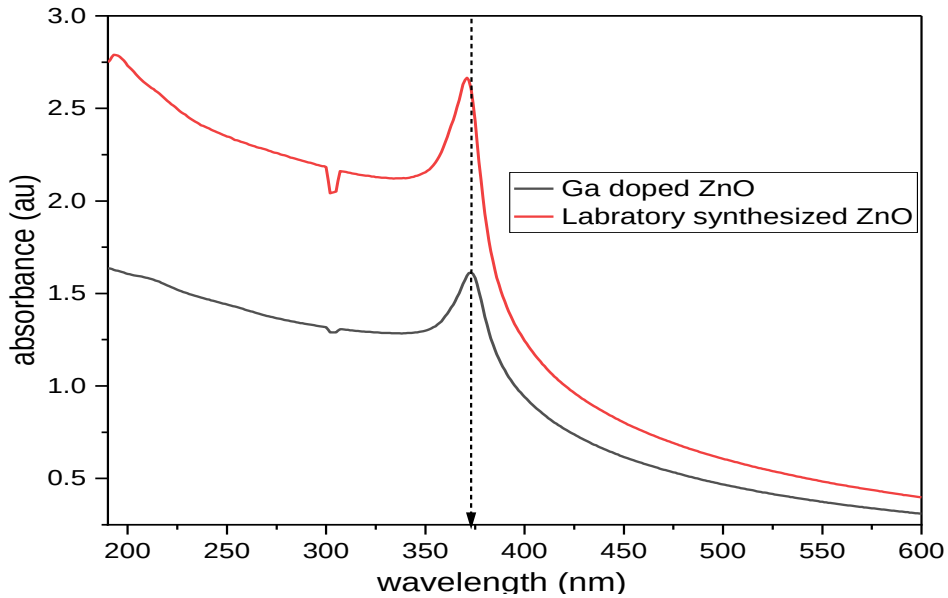

Figure 5.5 UV-Vis Spectroscopy for non-doped and Ga-doped ZnO NPs

5.3.6 TFT properties

To confirm the current transportation ability using obtained spray-coated NP layers, TFTs with MES-gate structure were demonstrated. Each TFT had a 450 m channel length and a 300 m gate width. The MESFET's gate current behaves similarly to that of a Schottky diode. The isolated work functions of the n-ZnO and gold (gate electrode) were very similar to one another at approximately 4.2 and 5.1 eV, resulting in the formation of a Schottky barrier along the channel[36]. For negative gate voltages, the Schottky barrier between the Au gate electrode and the ZnO NP layer was biased in the opposite way, and the gate current approximated the voltage independent Schottky junction saturation current. The depletion width of the Schottky contact between the metal gate electrode and the semiconductor determines the density of free charge carriers (and thus the conductivity of the semiconductor) in a MESFET device[37]. The output characteristics (I_D-V_{DS}) of fabricated TFTs are shown in **Fig. 5.6 (a), (b), (c), and (d).** The TFT channels layers were prepared with as-prepared ZnO, ZnO:Ga-open air, ZnO:Ga-N_2, and ZnO:Ga-O_2 layers, where the gate leakage current was sufficiently low in all conditions, on the order of 10^{-14} A. The I_D-V_{DS} results revealed that the drain current of Ga-doped ZnO NP layers (particularly in ZnO:Ga-open air) was significantly increased by at least 1000 times or greater compared with the as-prepared samples. The drain current was found to be decreased phenomenon in ZnO:Ga-N_2 (10^{-6}) and ZnO:Ga-O_2(10^{-7}), which is highly consistent with the resistivity behavior graph. This implies that the doped Ga atoms in the ZnO NPs act as activated donors, generating carriers and thereby lowering channel resistance. The variation of electric field-effect is clearly observed by changing the applied gate voltage (V_G) for all cases. Because of the depletion mode MESFET structure, the maximum drain current is obtained at the gate voltage is zero (V_G=0V), suggesting that the device is typically ON. Furthermore, when the negative terminal voltage (-V_G) is applied, the drain current gradually decreases, increasing the depletion region and inhibiting electron transport in the conduction layer. If the gate voltage is negative enough, the current will saturate, and the device will turn OFF. As a result of this electrical characterization, the ambient effect of our unique Ga-doping on ZnO-NPs was clearly observed.

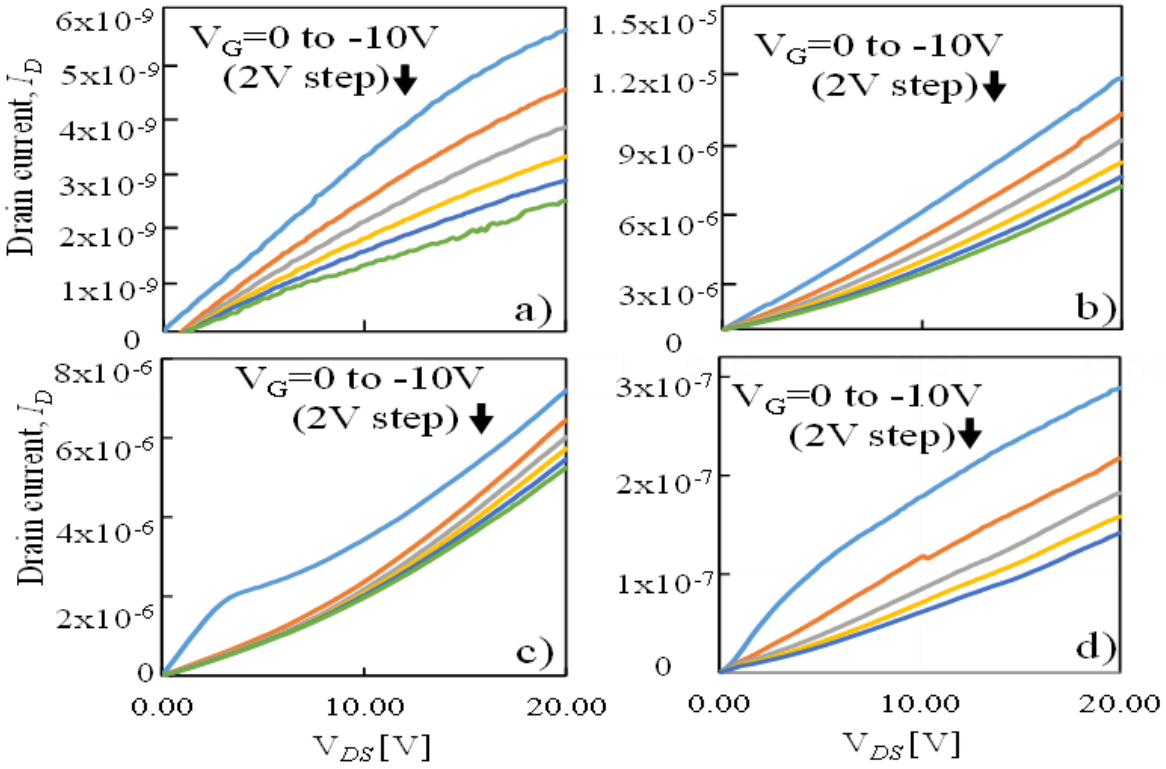

Figure 5.6 I_D–V_D characteristics of MESFETs consisting of channels prepared from (a) as-prepared ZnO, (b) ZnO:Ga-open air, (c) ZnO:Ga-N_2, and (d) ZnO:Ga-O_2. Referring [23].

5.4 Chapter Conclusions

Various atmospheric ambient was carried out during thermal diffusion-type Ga-doping processes on ZnO NPs. In our unique diffusion type Ga-doping process the ambient air and wet air conditions were found to be effective to achieve the low resistive ZnO NP layers. Humidity (H_2O) plays a key role in the improvement of layer properties in the manner of Ga diffusion. The impact of the ambient atmosphere was extensively outlined in our study throughout the PL and XRD analyses. These findings imply that the lowest sheet resistance was attributed to improved current transportation ability and the improved crystallinity was achieved due to the strong UV emission intensity. The current transportation ability can be dramatically improved by applying these ZnO:Ga NP layers to TFT channels. Our innovative Ga-doping into ZnO NPs technology, as well as their

spray coating method, are ideal for obtaining semiconducting NP layers for TFT applications.

5.5 References

[1] J. Yun, K. Cho, and S. Kim, "Nanoparticle-based flexible inverters with a vertical structure," *Thin Solid Films*, vol. 539, pp. 256–259, 2013, doi: 10.1016/j.tsf.2013.04.147.

[2] N. Chen *et al.*, "Application of Laser Treatment in MOS-TFT Active Layer Prepared by Solution Method," *Micromachines*, vol. 12, no. 12, p. 1496, 2021, doi: 10.3390/mi12121496.

[3] J. K. Saha, R. N. Bukke, N. N. Mude, and J. Jang, "Significant improvement of spray pyrolyzed ZnO thin film by precursor optimization for high mobility thin film transistors," *Sci. Rep.*, vol. 10, no. 1, pp. 1–11, 2020, doi: 10.1038/s41598-020-65938-6.

[4] H. Li *et al.*, "Bi-layer Channel AZO/ZnO Thin Film Transistors Fabricated by Atomic Layer Deposition Technique," *Nanoscale Res. Lett.*, vol. 12, no. 1, pp. 4–9, 2017, doi: 10.1186/s11671-017-1999-7.

[5] A. H. Farha, M. M. Ibrahim, and S. A. Mansour, "Ga-doped ZnO nanostructured powder for cool-nanopigment in environment applications," *Materials (Basel).*, vol. 13, no. 22, pp. 1–16, 2020, doi: 10.3390/ma13225152.

[6] A. M. Alsaad, A. A. Ahmad, I. A. Qattan, Q. M. Al-Bataineh, and Z. Albataineh, "Structural, optoelectrical, linear, and nonlinear optical characterizations of dip-synthesized undoped zno and group iii elements (B, al, ga, and in)-doped zno thin films," *Crystals*, vol. 10, no. 4, 2020, doi: 10.3390/cryst10040252.

[7] V. Şenay *et al.*, "ZnO thin film synthesis by reactive radio frequency magnetron sputtering," *Appl. Surf. Sci.*, vol. 318, pp. 2–5, 2014, doi: 10.1016/j.apsusc.2013.10.044.

[8] R. Mimouni, K. Boubaker, and M. Amlouk, "Investigation of structural and optical properties in Cobalt-Chromium co-doped ZnO thin films within the Lattice Compatibility Theory scope," *J. Alloys Compd.*, vol. 624, pp. 189–194, 2015, doi: 10.1016/j.jallcom.2014.11.016.

[9] D. Itohara, K. Shinohara, T. Yoshida, and Y. Fujita, "P-Channel and n-Channel Thin-Film-

Transistor Operation on Sprayed ZnO Nanoparticle Layers," *J. Nanomater.*, vol. 2016, no. Dc, 2016, doi: 10.1155/2016/8219326.

[10] K. Senthilkumar, O. Senthilkumar, S. Morito, T. Ohba, and Y. Fujita, "Synthesis of zinc oxide nanoparticles by dc arc dusty plasma," *J. Nanoparticle Res.*, vol. 14, no. 10, 2012, doi: 10.1007/s11051-012-1205-x.

[11] M. Khuili, N. Fazouan, H. A. El Makarim, G. El Halani, and E. H. Atmani, "Comparative first principles study of ZnO doped with group III elements," *J. Alloys Compd.*, vol. 688, pp. 368–375, 2016, doi: 10.1016/j.jallcom.2016.06.294.

[12] Z. Gao and P. Banerjee, "Review Article: Atomic layer deposition of doped ZnO films," *J. Vac. Sci. Technol. A*, vol. 37, no. 5, p. 050802, 2019, doi: 10.1116/1.5112777.

[13] A. Zaier, A. Meftah, A. Y. Jaber, A. A. Abdelaziz, and M. S. Aida, "Annealing effects on the structural, electrical and optical properties of ZnO thin films prepared by thermal evaporation technique," *J. King Saud Univ. - Sci.*, vol. 27, no. 4, pp. 356–360, 2015, doi: 10.1016/j.jksus.2015.04.007.

[14] J. K. Sheu, K. W. Shu, M. L. Lee, C. J. Tun, and G. C. Chi, "Effect of Thermal Annealing on Ga-Doped ZnO Films Prepared by Magnetron Sputtering," *J. Electrochem. Soc.*, vol. 154, no. 6, p. H521, 2007, doi: 10.1149/1.2721760.

[15] J. L. Tian, G. G. Wang, and H. Y. Zhang, "Effect of annealing atmosphere on the structural and optical properties of ZnO thin films on Si (100) substrates grown by atomic layer deposition," *J. Nano Res.*, vol. 37, pp. 92–98, 2016, doi: 10.4028/www.scientific.net/JNanoR.37.92.

[16] J. Dong, Q. Li, Z. Yi, D. Han, Y. Wang, and X. Zhang, "High-Performance ZnO Thin-Film Transistors on Flexible PET Substrates with a Maximum Process Temperature of 100 °c," *IEEE J. Electron Devices Soc.*, vol. 9, no. October 2020, pp. 10–13, 2021, doi: 10.1109/JEDS.2020.3034387.

[17] A. Abrutis, L. Silimavicius, V. Kubilius, T. Murauskas, Z. Saltyte, and V. Plausinaitiene, "Doped zinc oxide films grown by hot-wire chemical vapour deposition," *Thin Solid Films*, vol. 576, pp. 88–97, 2015, doi: 10.1016/j.tsf.2015.01.010.

[18] A. Illiberi, R. Scherpenborg, Y. Wu, F. Roozeboom, and P. Poodt, "Spatial atmospheric atomic layer deposition of alxzn1-xo," *ACS Appl. Mater. Interfaces*, vol. 5, no. 24, pp. 13124–13128, 2013, doi: 10.1021/am404137e.

[19] T. Ivanova, A. Harizanova, T. Koutzarova, and B. Vetruyen, “Optical and structural study of Ga and In co-doped ZnO films,” *Colloids Surfaces A Physicochem. Eng. Asp.*, vol. 532, no. April, pp. 357–362, 2017, doi: 10.1016/j.colsurfa.2017.04.068.

[20] C. Bhoomanee, P. Ruankhama, S. Choopun, A. Prathan, and D. Wongratanaphisan, “Effect of Al-doped zno for electron transporting layer in planar perovskite solar cells,” *Mater. Today Proc.*, vol. 17, pp. 1259–1267, 2019, doi: 10.1016/j.matpr.2019.06.014.

[21] T. Yoshida, I. M. Maruful, and Y. Fujita, “Trial of Ga-doping on ZnO nanoparticles by thermal treatment with Ga2O3 nanoparticles,” *e-Journal Surf. Sci. Nanotechnol.*, vol. 18, pp. 12–17, 2020, doi: 10.1380/EJSSNT.2020.12.

[22] Y. Fujita, K. Moriyama, Y. Hiragino, Y. Furubayashi, H. Hashimoto, and T. Yoshida, “Electroluminescence from nitrogen doped ZnO nanoparticles,” *Phys. Status Solidi Curr. Top. Solid State Phys.*, vol. 11, no. 7–8, pp. 1260–1262, 2014, doi: 10.1002/pssc.201300645.

[23] I.M.Maruful, Toshiyuki Yoshida, and Yasuhisa Fujita. 2022. "Effects of Ambience on Thermal-Diffusion Type Ga-Doping Process for ZnO Nanoparticles" *Coatings* 12, no. 1: 57. https://doi.org/10.3390/coatings12010057

[24] T. H. Chen and T. Y. Liao, “Influence of annealing temperature on the characteristics of Ti-Codoped GZO thin solid film,” *J. Nanomater.*, vol. 2013, 2013, doi: 10.1155/2013/502382.

[25] Z. Z. Li, Z. Z. Chen, W. Huang, S. H. Chang, and X. M. Ma, “The transparence comparison of Ga- and Al-doped ZnO thin films,” *Appl. Surf. Sci.*, vol. 257, no. 20, pp. 8486–8489, 2011, doi: 10.1016/j.apsusc.2011.04.138.

[26] M. C. Jun, S. U. Park, and J. H. Koh, “Comparative studies of Al-doped ZnO and Gadoped ZnO transparent conducting oxide thin films,” *Nanoscale Res. Lett.*, vol. 7, pp. 1–6, 2012, doi: 10.1186/1556-276X-7-639.

[27] E. Muchuweni, T. S. Sathiaraj, and H. Nyakotyo, “Synthesis and characterization of zinc oxide thin films for optoelectronic applications,” *Heliyon*, vol. 3, no. 4, p. e00285, 2017, doi: 10.1016/j.heliyon.2017.e00285.

[28] Y. X. Liu *et al.*, “Preferred orientation of ZnO nanoparticles formed by post-thermal annealing zinc implanted silica,” *Solid State Commun.*, vol. 121, no. 9–10, pp. 531–536, 2002, doi: 10.1016/S0038-1098(02)00006-6.

[29] Q. Yang, X. Zhang, X. Zhou, and S. Liang, “Growth of Ga-doped ZnO films by thermal oxidation with gallium and their optical properties,” *AIP Adv.*, vol. 7, no. 5, 2017, doi: 10.1063/1.4983483.

[30] B. N. Q. Trinh, T. D. Chien, N. Q. Hoa, and D. H. Minh, “Solution-processable zinc oxide based thin films with different aluminum doping concentrations,” *J. Sci. Adv. Mater. Devices*, vol. 5, no. 4, pp. 497–501, 2020, doi: 10.1016/j.jsamd.2020.08.006.

[31] E. Mosquera and J. E. Diosa, “Luminescence of ZnO/MgO phosphors,” *Optik (Stuttg).*, vol. 243, no. June, p. 167416, 2021, doi: 10.1016/j.ijleo.2021.167416.

[32] Ü. Özgür *et al.*, “A comprehensive review of ZnO materials and devices,” *J. Appl. Phys.*, vol. 98, no. 4, pp. 1–103, 2005, doi: 10.1063/1.1992666.

[33] W. Zhu *et al.*, “Analysis of defect luminescence in Ga-doped ZnO nanoparticles,” *Phys. Chem. Chem. Phys.*, vol. 18, no. 14, pp. 9586–9593, 2016, doi: 10.1039/c6cp00746e.

[34] T. K. Min, T. L. Yoon, C. A. Ling, S. Mahmud, T. L. Lim, and K. G. Saw, “Molecular dynamics simulations and photoluminescence measurements of annealed ZnO surfaces,” *Phys. E Low-Dimensional Syst. Nanostructures*, vol. 90, pp. 28–36, 2017, doi: 10.1016/j.physe.2017.03.005.

[35] A. Khorsand Zak, R. Razali, W. H. Abd Majid, and M. Darroudi, “Synthesis and characterization of a narrow size distribution of zinc oxide nanoparticles,” *Int. J. Nanomedicine*, vol. 6, no. 1, pp. 1399–1403, 2011, doi: 10.2147/ijn.s19693.

[36] L. J. Brillson and Y. Lu, “ZnO Schottky barriers and Ohmic contacts,” *J. Appl. Phys.*, vol. 109, no. 12, 2011, doi: 10.1063/1.3581173.

[37] D. Kälblein *et al.*, “Top-gate ZnO nanowire transistors and integrated circuits with ultrathin self-assembled monolayer gate dielectric,” *Nano Lett.*, vol. 11, no. 12, pp. 5309–5315, 2011, doi: 10.1021/nl202767h.

6. Concluding Remarks

The research presented in this thesis focused on the attributes of a thermal diffusion type Ga-doped ZnO NPs layer prepared by spray-coating technics, the NP layers was used to develop a highly conductive TFT channel layer for thin-film transistor operation. The fabricated Ga-doped ZnO NPs layer was examined in terms of morphological, structural, optical, and electrical properties. The research mainly investigates the impact of thermal atmosphere and temperature of Ga-doped ZnO NPs layer by concerning the crystallite size, defect analysis, and the diffusion mechanism to achieve the low resistive TFT channel layer. The structural measurement revealed that the crystal properties have been influenced by highly *a*-axis orientation after Ga-doping. Concerning the resistivity of NPs Layer, current conduction ability increased with a decrease of layer resistivity, which lead to the successful TFT operation in this dissertation.

As the first topic, the effect of Ga-doping into ZnO NPs depending on the annealing temperature was investigated with detailed effects of annealing temperature on electrical properties. It was found that the NPs annealed at 800°C effectively reduce the resistivity of NPs layer and the XPS analysis revealed that the Ga-doping was successfully achieved.

As the second topic, concerning to electrical properties of Ga-doped ZnO NP layers with structural and defects analysis was discussed. It was pointed out that the significance of crystallite size, crystallite boundary, and the low defect ratio with large exciton emission sufficiently reduce the resistivity on the sprayed NPs layer, resulting in the improved current transportation ability was achieved by the TFT measurement. It was stated clearly that the *a*-axis orientation of NPs layer reduces the contribution of crystallite boundary as well as increased crystallite size. The various native defects formed by the annealing atmosphere and or the doping-related materials were discussed. The reduction of defects and improved exciton emission imply the improvement of electrical conductivity by reducing the resistivity of NPs layer. These findings refer to two key parameters to consider while attempting to increase the performance of Ga-doped ZnO NPs layer deposited at 800°C, one is the preferred orientation of the NPs perpendicular to the *a*-axis on the surface to minimize the crystallite boundary and the other one is the variation of native defects induced by the thermal atmosphere and or the doping-related defects. It should be emphasized that annealing with high humidity for Ga-doping using our novel

thermal diffusion technique can effectively reduce the layer resistivity with improved optical, structural, and electrical properties.

For the practical application of Ga-doped ZnO NPs layer as Thin-film Transistor, low resistivity with enhanced electrical properties is required confirmed based on the above discussion. One of the crucial issues of ZnO-based TFT is low voltage application, that is, the resistivity of the NPs layer strictly inhibits the current conductivity of the channel layer which means that the high voltage should be applied to the device turn ON/OFF for high resistive channel layer TFTs. In order to overcome this issue, the influence of thermal temperature and thermal atmosphere with Ga-doping has been investigated in this thesis.

The findings from the research presented in this dissertation are likely to aid in the development of a variety of applications of Ga-doped ZnO NPs layers.